The Diabetes Drug Target MitoNEET Governs a Novel Trafficking Pathway to Rebuild an Fe-S Cluster into Cytosolic Aconitase/Iron Regulatory Protein 1

Ioana Ferecatu, Sergio Gonçalves, Marie-Pierre Golinelli-Cohen, Martin Clémancey, Alain Martelli, Sylvie Riquier, Eric Guittet, Jean-Marc Latour, Hélène Puccio, Jean-Claude Drapier, et al.

Cell Biology:

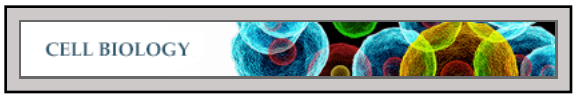

The Diabetes Drug Target MitoNEET Governs a Novel Trafficking Pathway to Rebuild an Fe-S Cluster into Cytosolic Aconitase/Iron Regulatory Protein 1

Ioana Ferecatu, Sergio Gonçalves, Marie-Pierre Golinelli-Cohen, Martin Clémancey, Alain Martelli, Sylvie Riquier, Eric Guittet, Jean-Marc Latour, Hélène Puccio, Jean-Claude Drapier, Ewen Lescop and Cécile Bouton

J. Biol. Chem. 2014, 289:28070-28086.
doi: 10.1074/jbc.M114.548438 originally published online July 10, 2014

THE JOURNAL OF BIOLOGICAL CHEMISTRY VOL. 289, NO. 41, pp. 28070–28086, October 10, 2014

The Diabetes Drug Target MitoNEET Governs a Novel Trafficking Pathway to Rebuild an Fe-S Cluster into Cytosolic Aconitase/Iron Regulatory Protein 1*

Received for publication, January 10, 2014, and in revised form, July 9, 2014 Published, JBC Papers in Press, July 10, 2014, DOI 10.1074/jbc.M114.548438

Ioana Ferecatu[‡], Sergio Gonçalves[‡], Marie-Pierre Golinelli-Cohen[‡§], Martin Clémancey[¶], Alain Martelli[‖‡‡§§¶¶], Sylvie Riquier[‡], Eric Guittet[‡], Jean-Marc Latour[¶], Hélène Puccio[‖**‡‡§§¶¶], Jean-Claude Drapier[‡], Ewen Lescop[‡], and Cécile Bouton[‡1]**

*From the [‡]Centre de Recherche de Gif, Institut de Chimie des Substances Naturelles, CNRS, 1 avenue de la Terrasse, 91190 Gif-sur-Yvette, France, the [¶]Direction des Sciences du Vivant, Institute of Life Sciences Research and Technologies, Chemistry and Biology of Metals Laboratory, UMR 5249 CEA-Université Grenoble I-CNRS/Equipe de Physicochimie des Métaux en Biologie, CEA-Grenoble, 17 rue des Martyrs, 38054 Grenoble Cedex 09, France, the [‖]Translational Medicine and Neurogenetics, Institut de Génétique et de Biologie Moléculaire et Cellulaire (IGBMC), F-67400 Illkirch, France, the **INSERM, U596, Illkirch, France, the [‡‡]CNRS, UMR7104, Illkirch, France, the [§§]Université de Strasbourg, F-67000 Strasbourg, France, the [¶¶]Collège de France, Chaire de Génétique Humaine, Illkirch, France, and the [§]Institut Jacques Monod, CNRS, UMR 7592, Université Paris Diderot, Sorbonne Paris Cité, 75205 Paris, France*

Background: MitoNEET is a mammalian iron-sulfur protein with the ability to transfer iron-sulfur (Fe-S) *in vitro*.
Results: MitoNEET conveys Fe-S from the mitochondrion to the cytosol and reactivates cytosolic iron regulatory protein 1 into an Fe-S aconitase.
Conclusion: A novel mitoNEET-dependent Fe-S repair pathway affects a key regulator of iron metabolism.
Significance: MitoNEET is the first mitochondrial protein found to be involved in mammalian cytosolic Fe-S repair.

In eukaryotes, mitochondrial iron-sulfur cluster (ISC), export and cytosolic iron-sulfur cluster assembly (CIA) machineries carry out biogenesis of iron-sulfur (Fe-S) clusters, which are critical for multiple essential cellular pathways. However, little is known about their export out of mitochondria. Here we show that Fe-S assembly of mitoNEET, the first identified Fe-S protein anchored in the mitochondrial outer membrane, strictly depends on ISC machineries and not on the CIA or CIAPIN1. We identify a dedicated ISC/export pathway in which augmenter of liver regeneration, a mitochondrial Mia40-dependent protein, is specific to mitoNEET maturation. When inserted, the Fe-S cluster confers mitoNEET folding and stability *in vitro* and *in vivo*. The holo-form of mitoNEET is resistant to NO and H_2O_2 and is capable of repairing oxidatively damaged Fe-S of iron regulatory protein 1 (IRP1), a master regulator of cellular iron that has recently been involved in the mitochondrial iron supply. Therefore, our findings point to IRP1 as the missing link to explain the function of mitoNEET in the control of mitochondrial iron homeostasis.

In mammals, iron-sulfur cluster (Fe-S) proteins assist vital biological processes such as enzymatic catalysis, DNA synthesis and repair, ribosome biogenesis, iron homeostasis, and heme synthesis (1). Biogenesis of these prosthetic centers is a complex process that is first carried out by the mitochondrial iron-sulfur cluster (ISC)[2] assembly machinery. Iron is taken into mitochondria by the two iron transporters mitoferrin 1 and 2 (MFRN-1 and MFRN-2) (2) and then assembled with inorganic sulfide produced from L-cysteine by the cysteine desulfurase NFS1-ISD11 complex to form a transient Fe-S on the ISCU scaffold protein. This step is controlled by frataxin, the protein lacking in Friedreich ataxia, the most common recessive ataxia in the Caucasian population (3). Early Fe-S assembly also requires the ferredoxin/ferredoxin reductase (FDX2/FDXR)-reducing system (4). Neosynthesized Fe-S are then transferred from ISCU to mitochondrial recipients, mainly Fe-S subunits of the respiratory chain complexes, with the help of the HSC20/HSPA9 chaperone system (5) and glutaredoxin 5 (6). Maturation of extramitochondrial Fe-S proteins is more elusive. It requires most components of the mitochondrial ISC assembly machinery, the cytosolic Fe-S assembly (CIA) machinery (7) and the still poorly characterized mitochondrial ISC export machinery. The only known components of the latter are the inner mitochondrial membrane transporter ABCb7 (8) and, very likely, both the Erv1p-mammalian orthologue ALR (9) and

* This work was supported by an ICSN-CNRS fellowship (to I. F.), by the Fondation de la Recherche Médicale (ING20101220983 to S. G.), and by the Agence Nationale de la Recherche (ANR-13-BSV8-0017-01).
[1] To whom correspondence should be addressed: Institut de Chimie des Substances Naturelles, UPR 2301-CNRS, 1 ave. de la Terrasse 91190, Gif-sur-Yvette, France. Tel.: 33-1-69-82-30-10; Fax: 33-1-69-07-72-47; E-mail: cecile.bouton@cnrs.fr.

[2] The abbreviations used are: ISC, iron-sulfur cluster; ISCU, iron-sulfur cluster assembly enzyme; CIA, cytosolic Fe-S assembly; ALR, Augmenter of Liver Regeneration; mNT, mitoNEET; OMM, outer mitochondrial membrane; FDX, ferredoxin; FAC, ferric ammonium citrate; DFO, desferrioxamine; SIH, salicylaldehyde isonicotinoyl hydrazone; DETA-NO, diethylenetriamine NONOate; DEA-NO, diethylamine NONOate; Tricine, *N*-[2-hydroxy-1,1-bis(hydroxymethyl)ethyl]glycine; GPAT, glutamine phosphoribosylpyrophosphate aminotransferase; NARFL, nuclear prelamin A recognition factor-like; VDAC, voltage-dependent anion channel; NC, negative control; IMS, intermembrane space; ROS, reactive oxygen species; TCI, Triple Resonance Probes; HSQC, Heteronuclear Single Quantum Coherence; SOFAST-HMQC, SOFAST-Heteronuclear Multiple-Quantum Correlation.

glutathione (10, 11). To date, the exact mechanism of transfer of preassembled Fe-S from mitochondria to the cytosol is not understood.

MitoNEET (mNT) is the first identified Fe-S protein of the mammalian outer mitochondrial membrane (OMM). The function of mNT remains unknown, but recent mouse model studies have shown that its overexpression promotes lipid accumulation in adipocytes while preserving insulin sensitivity in obese mice (12). Moreover, mNT has been acknowledged as a novel potential pharmacological target of pioglitazone, a member of the thiazolidinedione class used in the treatment of type 2 diabetes (13), although this finding has recently been called into question (14).

Crystallographic studies revealed that mNT dimerizes and accommodates one [2Fe-2S] cluster per monomer, adding mNT to the growing list of newly identified Fe-S proteins (15–18). This 13-kDa protein is anchored to the OMM by its 32-amino acid N terminus with the C-terminal Fe-S binding domain oriented toward the cytosol (19). The crystal structure of mNT further shows an unusual cluster ligand environment because each [2Fe-2S] is coordinated by three cysteines (Cys-72, Cys-74, and Cys-83) and one histidine (His-87) in a CDGSH domain, and its stability decreases at a lower pH (17). Finally, a recent study showed that human mNT is capable of Fe-S transfer to a bacterial apo-ferredoxin (FDX) *in vitro* (20). However, the physiological recipients and the conditions of mNT Fe-S transfer in living cells have not yet been identified.

In this study, we analyzed the maturation pathway of mNT Fe-S and show that its assembly requires a specific HSC20/ABCb7/ALR branch pathway with no connection to the CIA machinery. We also provide evidence for a role of mNT in the Fe-S repair of cytosolic aconitase/IRP1, a critical regulator of genes important for iron homeostasis and oxygen sensing.

EXPERIMENTAL PROCEDURES

Animals—Mice with a specific deletion of the *Fxn* gene in the heart (MCK-*Fxn*) and liver (ALB-*Fxn*) were generated as described previously (3, 21). Mice bearing the *Abcb7* conditional allele were provided by Mark D. Fleming (Children's Hospital, Boston, MA). Mice with a specific deletion of *Abcb7* in the liver (ALB-*Abcb7*) were obtained as described previously (22). All methods employed in this work are in accordance with the Guide for the Care and Use of Laboratory Animals published by the National Institutes of Health (NIH Publication No. 85-23, revised 1996).

Cell Culture and Treatment—HeLa and liver hepatocellular carcinoma cells (HepG2) were cultured in DMEM (Sigma) containing 4.5 g/liter glucose and 1 mM stable L-glutamine and supplemented with 1% penicillin-streptomycin and 10% fetal bovine serum (Lonza) under 5% CO_2 and a humidified atmosphere. HeLa cells were seeded at 3.5×10^5 cells/cm^2, incubated overnight, and transfected with siRNA duplexes with INTERFERin^{TM} (Polyplus Transfection) according to the recommendations of the manufacturer (Ozyme). When specified, cells were retransfected every 3 days. Carbonyl cyanide 3-chlorophenylhydrazone (200 μM), ferric ammonium citrate (FAC, 100 μM), desferrioxamine (DFO, 50 μM) and Z-Leu-Leu-Leu-al (MG132, 25 μM) were from Sigma. Lactacystin (10 μM) was from Calbiochem. Salicylaldehyde isonicotinoyl hydrazone (SIH, 50 μM) was a gift from P. Ponka (McGill University, Montreal, Quebec, Canada). For NO and H_2O_2 challenge studies, untransfected or siRNA-transfected HeLa cells were cultured for 72 h and exposed or not exposed to diethylenetriamine NONOate (DETA-NO, 250 μM) for 16 h or H_2O_2 (100 and 150 μM) for 1 h. The DETA-NO concentration was determined by absorbance at 252 nm ($\epsilon = 7640\ M^{-1}\ cm^{-1}$). For recovery after NO or H_2O_2 exposure, cells were washed extensively and incubated for an additional 1–24 h in fresh cell culture medium. For *in vitro* NO exposure, holo-mNT was incubated with spermine-NO complex (600 μM) for 3 h or H_2O_2 (100 μM) for 3 h in a buffer containing 100 mM NaCl, 50 mM Tris-HCl (pH 7). NO donors were from Cayman Chemical.

Immunoblots and Quantitative Real-time PCR Analysis—Equal amounts of proteins (40 μg) were separated on SDS-Tricine-PAGE and transferred to PVDF membranes. The primary antibodies used were anti-ALR (Sigma, catalog no. HPA041227), anti-β-actin (Sigma, catalog no. A5441), anti-β-tubulin (Cell Signaling Technology, catalog no. 2146), anti-GPAT (IGBMC, Illkirch, France), anti-HSC20 (Sigma, catalog no. HPA018447), anti-IRP1 (Agro-Bio, La Ferté Saint-Aubon, France), anti-IRP2 (a gift from Dr. J. M. Moulis, CEA, Grenoble, France), anti-ISCU (Proteintech, catalog no. 14812-1-AP), anti-m-aconitase (a gift from Dr. R. B. Franklin, University of Baltimore, Baltimore, MD), anti-mNT (designed by Eurogentec), anti-NARFL (Sigma, catalog no. HPA040851), anti-NDUFS3 (MitoScience, catalog no. MS112), anti-NFS1 (Agro-Bio), anti-NUBP1 (Sigma, catalog no. HPA041656), anti-CIAPIN1 (Sigma, catalog no. HPA042182), anti-RIESKE (MitoScience, catalog no. MS305), anti-MIA40 (a gift from Prof. Pfanner, University of Freiburg, Freiburg, Germany), anti-vinculin (Sigma, catalog no. V9131), and anti-VDAC (a gift from Dr. C. Brenner, INSERM U769, University of Paris Sud, Paris, France). Secondary antibodies used were anti-mouse, anti-rabbit, and anti-chicken fluorescent IRDye 800CW (Li-Cor). Membranes were scanned with an Odyssey® imaging system (Li-Cor), and quantitation was performed using Li-Cor Odyssey software. In some gel images, non-relevant or unnecessary lines were removed and demarcated clearly by using boxes.

Total RNA from cells was extracted using the SV total RNA isolation system according to the protocol of the manufacturer (Promega), and the reverse transcription (1 μg of total RNA) was performed using the high-capacity cDNA archive kit (Applied Biosystems). Quantitative real-time PCR was performed using the FastStart DNA Master Plus SYBR Green I kit and the Roche Lightcycler system (Roche Applied Sciences). Primer sequences used were Hu-*mNT*, 5′-CTAGTGCACACGCCTTGCAA-3′ (forward) and 5′-CTGCTGCGATCCATTCAACTC-3′) (reverse); Hu-*IscU2*, 5′-CCCGACTCTATCACAAGAAGGTTG-3′ (forward) and 5′-CATGCTGGAGCCCCCAC-3′) (reverse); and Hu-*Abcb7*, 5′-GCTCGAGCCTACCAGCAGATT-3′ (forward) and 5′-GGCCTGTCTTTGGGCCAC-3′ (reverse). Sequence-specific primers were designed to span intron-exon boundaries to generate amplicons of ~100 bp. Values were normalized to 18 S rRNA.

Transfection and Preparation of Cell and Tissue Extracts—The following siRNA duplexes were from Life Technologies®: CISD1 (*mNT*-0, catalog no. s31650; *mNT*-1, catalog no. s31651), *Iscu*-2 (catalog no. s23909), *Nfs1* (catalog no. s17265), *Mfrn*-2 (catalog no. s37872), *Hsc20* (catalog no. s45405), *Abcb7* (catalog no. 117249), *Alr* (*Alr*-3, catalog no. s5703; *Alr*-4, catalog no. s5704), *Nupb1* (catalog no. s9288), *Narfl* (catalog no. s34746), *ciapin1* (catalog no. s32591), and negative control (catalog no. 4390843). They were used at final concentrations ranging from 1–10 nM. The pcDNA3-GPAT-C1F vector containing a noncleavable GPAT precursor was used as described previously (23). Total protein extracts from human cell lines were obtained by harvesting cells in Laemmli buffer (0.06 M Tris-HCl (pH 6.8), 10% glycerol, 2% SDS, and protease inhibitors (Calbiochem)). Total protein extracts from mouse heart were obtained as described previously (24), except for the final lysis, which was performed in 2.5× Laemmli buffer.

Mitochondrion-enriched fractions were prepared using a conventional differential centrifugation procedure as described before (25). The digitonin (0.007%) method for preparing mitochondrial and cytosolic fractions was also used as described previously (26). Protein concentrations were determined using the BCA method.

Cell Viability—Cell viability was determined microscopically by trypan blue exclusion. Viable cell number was reported as a percentage of negative control (NC) siRNA-transfected cells. Cells were also analyzed for hallmarks of mitochondrial depolarization by using the membrane-permeable JC-1 dye, and flow cytometry was performed on an FC500 Beckman Coulter instrument. Mitochondrial uncoupler carbonyl cyanide 3-chlorophenylhydrazone-treated cells were used as a positive control.

In vitro Fe-S Transfer to Recipient Proteins and Aconitase Activity—Human apo-IRP1 was generated by treatment of 290 μM holo-IRP1 with 7 mM DEA-NO in 20 mM Hepes (pH 7.3), 0.2 mM citrate, and 30 mM ammonium acetate for 1 h at 29 °C in a glove box and purification on a microbiospin equilibrated with 10 mM Hepes (pH 7.6), 40 mM KCl, and 3 mM $MgCl_2$. Apo-IRP1 was preincubated with 5 mM DTT for 30 min at room temperature under anaerobic conditions. Then, purified mNT_{44-108} (100 μM of holo-protein or disassembled protein) was incubated in an anaerobic atmosphere at 25 °C with apo-IRP1 (25 μM) in 100 mM BisTris (pH 6.2), 100 mM NaCl, and 5 mM DTT. At the indicated times, aliquots of the transfer reaction were used to measure aconitase activity. Disassembled mNT was prepared by incubation of the protein in buffer containing 100 mM BisTris pH 6.2 and 100 mM NaCl at 65 °C for 10 min. Chemical reconstitution of the aconitase Fe-S cluster was performed in the same buffer as the one used for the transfer reaction with 250 μM Na_2S and Mohr's salt for 1 h at 25 °C under anaerobic conditions. The transfer reaction, using *Escherichia coli* FDX as the recipient protein, was performed similarly at 20 °C with equal concentrations of holo-mNT and apo-*E. coli* FDX. UV-visible absorption spectra were recorded from 350–550 nm (Varian Cary 100). In parallel, the transfer reaction was followed by differential migration of mNT and FDX holo- and apo-forms on native PAGE and Coomassie staining. Experiments on mNT stability were performed using 100 μM oxidized mNT in 100 mM BisTris (pH 6.2) with 100 mM NaCl and 5 mM DTT at 25 °C under anaerobic conditions. The absorbance at 460 nm was monitored over time, and the percentage cluster loss was calculated using the absorbances at 460 nm at time 0 and at times 30, 65, and 150 min.

Aconitase activity was measured as described previously (26). For mitochondrial aconitase activity, the lysis and enzymatic activity measurement steps were performed under an anaerobic atmosphere using buffers flushed with nitrogen gas.

Purification and Preparation of Protein Samples—Recombinant human mNT missing the 43 N-terminal amino acids was expressed from the pET22b and pET28a vectors in BL21(DE3) cells with the addition of 0.4 mM isopropyl 1-thio-β-D-galactopyranoside. Cells were cultured at 22 °C for 20 h in the presence of 400 μM $FeCl_3$ and then harvested for purification steps. The cleared lysate was applied to an nickel-nitrilotriacetic acid column on an Akta FPLC instrument (GE Healthcare). When required, a protease cleavage of the His tag was performed at this semipurification step using thrombin. The mNT fractions were further purified on a HiLoad 16/60 Superdex 75 size exclusion column (GE Healthcare). The mNT fractions from the size exclusion chromatography were pooled and concentrated to 4 mg/ml. Degassed buffers were used during the purification steps. Protein purity was assessed to be >99% using SDS-PAGE with an optical $A_{280\ nm}/A_{458\ nm}$ ratio near 2.3.

Two recombinant preparations of mNT (44–108) were finally obtained, one containing eight additional C-terminal residues derived from the His tag (LEHHHHHH) and the other containing three additional N-terminal residues derived from the thrombin cleavage site (GSH).

For NMR analyses, expression of mNT_{44-108} was performed on a 1-L scale in M9 minimal medium (containing 0.001% thiamine-HCl and 10 μM $FeCl_3$) supplemented with 1.0 g of $^{15}NH_4Cl$ and 4.0 g of [^{13}C]D-glucose as the sole nitrogen and carbon sources. For Mössbauer analysis, expression of mNT_{33-108} missing the 32 N-terminal amino acids (using the pET28a-mNT_{33-108} construct) was performed in M9 minimal medium supplemented with ^{57}Fe-enriched ferric chloride. The N-terminal His tag of purified mNT_{33-108} was removed efficiently using thrombin.

The *E. coli* apo-ferredoxin (full-length construct in pET21, a gift from Dr. S. Ollagnier de Choudens, Grenoble, France) was expressed and purified as described previously (27). The untreated and NO-treated IRP1 was a gift from Dr. J.-M. Moulis (CEA Grenoble, France).

Mitochondrial aconitase from a porcine heart was from Sigma. 100 mg was dissolved in 25 mM Hepes (pH 7.8) and loaded on a HiScreen Capto Q ImpRes column (GE Healthcare). Proteins were eluted with a linear NaCl gradient (0–1 M). Fractions containing aconitase were pooled and concentrated, and then the protein concentration was determined. Aconitase was reactivated by incubation for 1 h at room temperature under anaerobic conditions with 5× Mohr's salt and Na_2S and then loaded on a NAP-5 gel filtration column equilibrated with 25 mM Hepes (pH 7.8) and 100 mM NaCl.

Mössbauer and NMR Spectroscopy—Mössbauer spectra of purified ^{57}Fe-labeled mNT_{33-108} in 50 mM phosphate (pH 8.0), 50 mM NaCl were recorded at 4.2 K on a low-field Mössbauer

spectrometer equipped with a Janis SVT-400 cryostat and weak field permanent magnets. The spectrometer was operated in a constant acceleration mode in transmission geometry (28). The isomer shifts were referenced against that of room temperature metallic iron foil. Data were analyzed with the WMOSS program (WEB Research, Edina, MN).

NMR experiments were carried out using a Bruker AVANCE 600-MHz spectrometer equipped with a TCI cryoprobe. Two-dimensional ^{1}H-^{15}N correlation HSQC spectra were obtained on a 250 μM His-tagged ^{13}C,^{15}N-labeled holo-mNT$_{44-108}$ protein sample at 298 K in 50 mM sodium phosphate (pH 8.0), 50 mM NaCl.

In Vitro Fe-S Reconstitution—Iron and sulfur incorporation into apo-mNT (44–108) was carried out by the addition of 10 mM DTT, 500 μM $[NH_4]_2Fe[SO4]_2$ and 500 μM sodium sulfide to 1.13 mg of purified $^{15}N/^{13}C$ double-labeled apo-mNT in 2.5 ml of 50 mM sodium phosphate (pH 8.0), 50 mM NaCl. All reactions were carried out in an anaerobic glove box (Jacomex, O_2 <9 ppm). After 5 h at room temperature, the protein was desalted on a NAP-5 column (Amersham Biosciences) and analyzed by UV-visible and NMR spectroscopy.

Statistical Analysis—All results are presented as mean ± S.D. of at least three independent experiments. Data were analyzed using one-way analysis of variance. Student-Newman-Keuls test was used for all pairwise comparisons of mean responses among the different treatment groups (SigmaStat). Two-tailed Student's *t* test was performed for all multiple pair comparisons. Differences between groups were considered significant if the *p* value was less than 0.05.

RESULTS

Cellular Fe-S Cluster Availability Ensures Stability and Proper Folding of mNT—Biophysical studies support the presence of a [2Fe-2S] prosthetic group in purified recombinant mNT (15–18), but evidence in living cells is still lacking. Therefore, we analyzed protein stability in two different human cell types, *i.e.* HeLa and HepG2 cells, grown under conditions that strongly reduce Fe-S biogenesis. First, cells were exposed to the lipophilic SIH iron chelator. Iron deficiency significantly decreased mNT at the protein level in both total extracts and mitochondria-enriched fractions (Fig. 1*A*). Time course experiments (Fig. 1*B*) demonstrated that the mNT protein level decreased within 16 h and was no longer detectable after 48 h upon iron starvation induced by SIH or by the iron chelator DFO. No difference in mNT mRNA levels upon exposure to elevated FAC levels or depletion of cellular iron (DFO and SIH) was detected (data not shown). Moreover, we observed that the decrease in mNT protein level induced by DFO or SIH was prevented significantly by addition of the proteasome inhibitors MG132 or lactacystin (not shown) in both total extracts (Fig. 1*C*) and mitochondrion-enriched fractions (Fig. 1*D*), demonstrating a mechanism involving protein degradation. Then, using siRNA, we depleted the mitochondrial scaffold isoform ISCU, an essential component for Fe-S cluster assembly. mNT was decreased markedly after 2 days of *Iscu* knockdown and disappeared at 6 days without modulation of its transcript (Figs. 2, *A* and *B*). Again, this decrease was prevented by lactacystin treatment (Fig. 2*C*). We also examined the *in vivo* mNT protein level in conditional mouse models of Friedreich ataxia in which frataxin has been deleted specifically in the heart and liver (3). In both cases, we observed a 55–75% reduction of mNT compared with tissues from control mice of the same age (Fig. 2*D*). Together, these results demonstrate that, under conditions of sustained impairment of ISC biogenesis, endogenous mNT is targeted for proteasomal degradation.

Finally, we investigated the mechanism of disassembly/reassembly of mNT Fe-S *in vitro* by NMR and UV-visible spectroscopy. The folded ^{15}N-labeled holo-mNT at pH 8 was characterized by a well dispersed ^{15}N SOFAST-HMQC spectrum and a $[2Fe\text{-}2S]^{2+}$ cluster absorbance peak at 458 nm (Fig. 3*A*, *left*). Mössbauer spectra of ^{57}Fe-labeled holo-mNT confirmed the arrangement of a $[2Fe\text{-}2S]^{2+}$ bound to three cysteines and one histidine (Fig. 3*B*). Twenty-four hours after a pH jump from 8 to 6, the protein lost both the cluster and its structured state (Fig. 3*A*, *center*). The mostly unstructured apo-mNT was then subjected to Fe-S cluster reconstitution in the presence of iron, sulfide, and DTT under anaerobic conditions. After 5 h at 4 °C, a red color developed, and the spectroscopic properties of the isolated protein were quasi-identical to those of the initial holo-mNT (Fig. 3*A*, *right*). These data demonstrate that mNT can cycle *in vitro* between a well folded holo-form and a highly unfolded apo-form just by insertion/disassembly/reinsertion of the Fe-S cluster.

The iron and Sulfur Atoms of mNT Fe-S Originate from Mitochondria—To identify the origin of mNT Fe-S, we took advantage of mNT degradation after a prolonged absence of its cluster (Fig. 1). Knockdown of the cysteine desulfurase NFS1, the mitochondrial sulfur donor, resulted in progressive mNT protein loss from 6–13 days (Fig. 4*A*, *lanes 5*, *6*, *9*, and *13*). The initial amount of mNT was then recovered when endogenous NFS1 returned to its basal level expression after transient depletion (Fig. 4*A*, compare *lanes 9*, *10*, and *11*). Iron is imported into the mitochondrial matrix by MFRN-1 and MFRN-2. Because only MFRN-2 shows ubiquitous expression, it was depleted in HeLa cells, which led to decreased levels of mNT protein (Fig. 4*B*). Furthermore, addition of FAC to *Mfrn-2* silenced cells increased cytosolic iron concentrations, as indicated by the iron-mediated loss of IRP2 protein (Fig. 4*C*) (29), but did not rescue mNT loss (Fig. 4*C*, compare *lanes 3* and *4*). Therefore, mNT Fe-S originates only from mitochondrially derived Fe and inorganic sulfide.

Maturation of the mNT Fe-S Cluster Is Mediated by a Specific Mitochondrial HSC20/ABCb7/ALR Branch Pathway and Not by the CIA—The mitochondrial heat shock cognate protein HSC20 is thought to act in a later step of the Fe-S pathway by triggering Fe-S release from ISCU (5, 30, 31). As shown in Fig. 4*D*, *Hsc20* silencing resulted in a conspicuous decrease in mNT protein level. The next step toward mNT maturation implies the transport of Fe-S or other, yet unidentified related compounds from the ISC machinery to the intermembrane space (IMS) across the inner mitochondrial membrane. As shown in Fig. 4*E*, gene knockdown of the inner mitochondrial membrane *Abcb7* exporter (8) resulted in a strong decrease of mNT protein level. These findings were also confirmed *in vivo* with $Abcb7^{lv/Y}$ mice (Fig. 4*F*, *left panel*), a conditional mouse model whose expression of *Abcb7* is specifically deleted in the liver

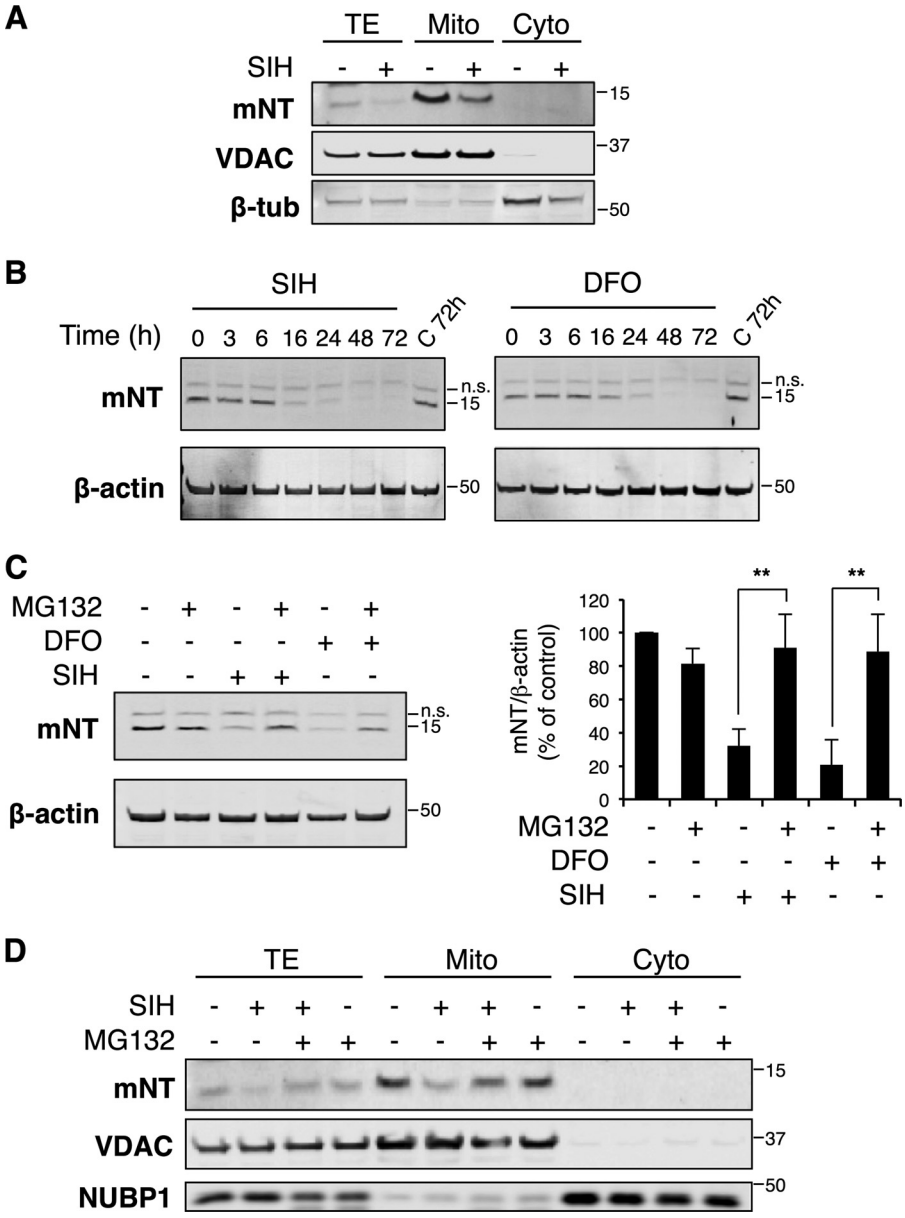

FIGURE 1. **Regulation of the endogenous mNT level upon cellular iron availability.** *A*, human HepG2 cells were incubated in the presence SIH for 24 h or not incubated. Western blotting was carried out to detect mNT protein in total protein extracts (*TE*) and mitochondrial (*Mito*) and cytosolic (*Cyto*) fractions. Anti-VDAC and -β-tubulin (*β-tub*) antibodies were used as mitochondrial and cytosolic markers, respectively. *B*, total lysates from untreated HeLa cells or after treatment with DFO or SIH were subjected to time course immunoblot analysis for detection of mNT protein. β-Actin was used as a loading control (*C*). *n.s.*, nonspecific. *C*, immunoblot analysis of mNT protein levels in untreated or DFO- or SIH-treated HeLa cells for 22 h in the presence of or without MG132. The histogram in the *right panel* represents the relative level of mNT determined by immunoblot analysis, which was expressed as the percentage of control untreated cells (means ± S.D.) after normalization using β-actin. **, $p < 0.001$ ($n = 4$). *D*, HepG2 cells were cultured in the presence or absence of SIH for 16 h with or without MG132. mNT protein levels were analyzed by immunoblot of total extracts and mitochondrial and cytosolic fractions. Fraction purity was assessed by immunoblot analysis with antibodies against VDAC and NUBP1 as mitochondrial and cytosolic markers, respectively.

(22). The protein level of the CIA scaffold NARFL, whose apoform is known to be highly sensitive to degradation (32), was also decreased clearly in *Abcb7*-depleted liver (Fig. 4*F*, *left panel*) as well as in *Hsc20*-depleted cells (Fig. 4*F*, *right panel*). These results show that, up to the selective inner mitochondrial membrane, mNT follows the same pathway for its maturation as other known cytosolic Fe-S proteins.

Given that mNT is located at the OMM, we then asked whether mNT accommodates its Fe-S prior to delivering it to the CIA. As shown in Fig. 5*A*, depletion of mNT did not affect NARFL expression even after 9 days of silencing, whereas the depletion of ISCU led to NARFL protein loss as expected (32). Furthermore, depletion of the essential CIA components NUBP1 and NARFL had no effect on mNT stability but led to loss of GPAT, a cytosolic [4Fe-4S] enzyme (Fig. 5*B*). These results show that mNT is not a relay between the ABCb7 exporter and the CIA for the maturation of extramitochondrial Fe-S proteins and that mNT does not receive its cluster from the CIA, implying the existence of a CIA-independent pathway downstream of the ABCb7 exporter for its maturation. In the IMS, the sulfhydryl oxidase ALR, a functional human orthologue of the yeast Erv1p, has been proposed to be a relay in

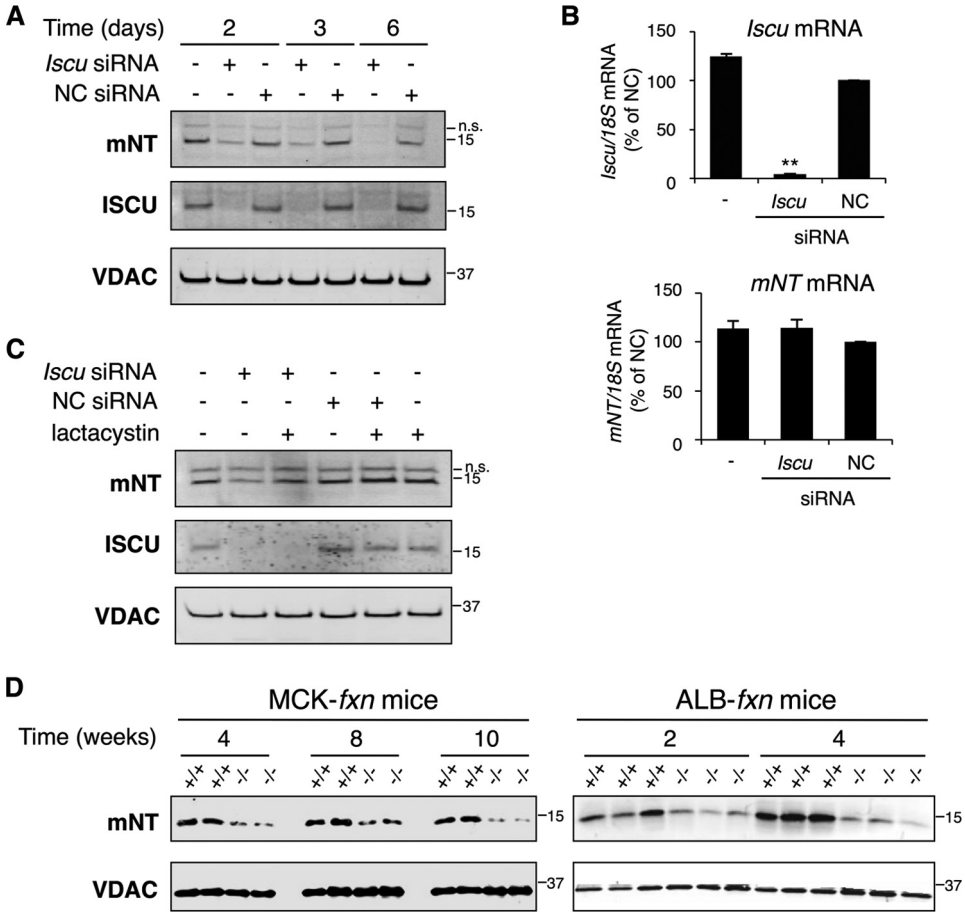

FIGURE 2. **Regulation of the mNT level upon a defect in mitochondrial ISC assembly.** *A*, HeLa cells were transfected with *Iscu* or NC siRNA for the indicated times. The mNT and ISCU protein levels were determined by immunoblotting. VDAC is shown as a loading control. *n.s.*, nonspecific. *B*, mRNA levels of *Iscu* (*top panel*) and *mNT* (*bottom panel*) were determined by quantitative RT-PCR performed 24 h after transfection. Data are normalized to 18 S ribosomal mRNA levels and represented as a percentage of NC ± S.D. **, $p < 0.001$ ($n = 3$). *C*, HeLa cells were either left untransfected or transfected with *Iscu* or NC siRNA for 2 days and then incubated in the presence of or without lactacystin for an additional 22 h. Immunoblotting was carried out to determine mNT, ISCU, and VDAC protein levels in total extracts. *D*, total protein extracts from the hearts of control (+/+) and *frataxin* deletion (−/−) mice in the MCK mouse model (*left panel*) and from the livers of the ALB mutant mice (*right panel*) were analyzed at the indicated number of weeks by immunoblotting using anti-mNT and anti-VDAC antibodies.

general Fe-S assembly of extramitochondrial recipient proteins (9). Unexpectedly, we observed that levels of NARFL and GPAT remained stable in ALR-deficient cells (Fig. 5*C*, *top panel*), whereas the mNT level was clearly reduced (Fig. 5*C*, *bottom panel*). ALR is a multifunctional protein also involved in import of cysteine-containing proteins (*e.g.* Tim and Cox proteins), which, in turn, may affect respiratory chain assembly (33). Therefore, we asked whether ALR-dependent mNT maturation could result from an impairment of ALR-dependent mNT import to mitochondria. To solve this issue, MG132 was used to allow the accumulation of neosynthesized mNT in ALR-depleted cells, and the subcellular localization of mNT was determined. As shown in Fig. 5*D*, the newly synthesized mNT, upon ALR deficiency, was found exclusively in the mitochondrial fraction and was totally absent from the cytosol (compare *lanes 4* and *8*). We also observed that the mitochondrial membrane potential was unaffected in ALR-depleted cells (data not shown), suggesting that the function of ALR in mitochondrial import, which may affect respiratory chain assembly, is not involved in mNT maturation.

Extramitochondrial Fe-S proteins, whose maturation does not require the CIA, are few in number (34, 35). Among them, Dre2, the yeast homolog of human CIAPIN1, which may exhibit two subcellular locations (IMS and cytosol) (36, 37), plays an important role as an early component of the CIA machinery (35, 37). Therefore, we investigated whether CIAPIN1 contributes to mNT maturation. As shown in Fig. 6, depletion of human CIAPIN1, which is mainly expressed in the cytosol in mammalian cells (Fig. 6*A*), did not change mNT abundance, whereas it led to progressive loss of NARFL and GPAT (Fig. 6*B*). These data suggest that CIAPIN1 is not involved in the specific branch maturation pathway of mNT but, rather, acts as an early component of the CIA machinery.

Taken together, these results demonstrate the existence of a bifurcation in the Fe-S biogenesis pathway at the IMS. One branch involving a function of ALR different from that implicated in mitochondrial import is dedicated to the CIA-independent maturation of mNT and another one, independent of ALR and mNT, involves the classic CIA pathway.

mNT Mediates Fe-S Cluster Repair of Human Cytosolic Aconitase/IRP1 after NO and H_2O_2 Exposure—Despite the fact that mNT is not a relay between ABCb7 and the CIA, we wondered whether it could deliver its Fe-S to cytosolic recipients. As shown in Fig. 7, *A* and *B*, mNT knockdown did not affect the

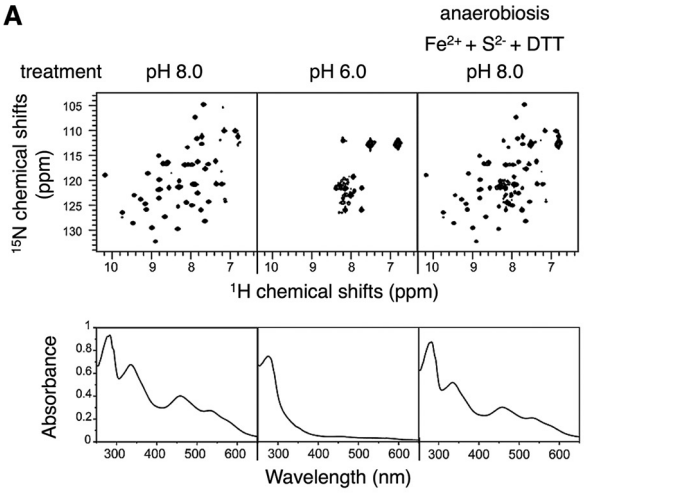

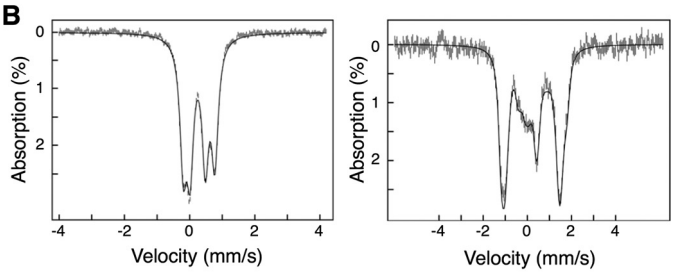

	Fe site	δ (mm.s^{-1})	ΔE_Q (mm.s^{-1})
mNT [2Fe-2S]$^{2+}$	1	0.26	0.47
	2	0.30	0.96
*IscU [2Fe-2S]$^{2+}$	1	0.27	0.66
	2	0.32	0.94

* data from (42)

FIGURE 3. **mNT unfolding and refolding upon Fe-S release and reassembly.** *A*, *in vitro* disassembly and reconstitution of mNT Fe-S clusters followed by NMR and UV-visible spectroscopy. *Top panel* (*left to right*), ^{15}N SOFAST-HMQC NMR spectra of a 250 μM His-tagged ^{13}C,^{15}N-labeled holo-mNT$_{44-108}$ at pH 8.0 after cluster release at pH 6.0 for 24 h under aerobic conditions (*center*) and after cluster reconstitution at pH 8.0 (*right*), respectively. All spectra were obtained at 298 K in 50 mM sodium phosphate (pH 8.0), 50 mM NaCl. Below each NMR spectrum the UV-visible absorption spectra recorded under the same conditions (*bottom panel*) are shown. *B*, Mössbauer spectrum of 1 mM ^{57}Fe-labeled holo-mNT$_{33-108}$ recorded at 4.2 K with a field of 60 mT (*top panel*, *left*) applied parallel to the γ beam. The *hatched bars* correspond to the experimental data and the *solid line* to the simulation with the parameters specified in the text. The spectrum is composed of two quadrupole doublets with an isomer shift (δ) and quadrupole splitting (ΔE_Q) very similar to those of the Mössbauer spectrum (4.2 K, 50 mT applied field parallel to γ radiation) of 2×[^{57}Fe-S]$^{2+}$ bacterial IscU (site 1, δ = 0.27 mm/s (*1*), ΔE_Q = 0.66 (*2*) mm/s; site 2, δ = 0.32 (*1*) mm/s, ΔE_Q = 0.94 (*2*) mm/s (42)). The spectrum of human mNT$_{33-108}$ recorded at 4.2 K under a field of 7 T (*right*) applied parallel to the γ beam confirmed the S = 0 ground state of the cluster.

maturation of the cytosolic Fe-S GPAT and had a moderate but significant effect on the cytosolic Fe-S aconitase. In addition, mNT knockdown in HeLa cells did not alter the mitochondrial membrane potential ($\Delta\Psi$m), which is needed for the export of a poorly defined sulfur-containing compound X (1) to cytosolic proteins (Fig. 7*C*). Moreover, mNT depletion did not affect protein levels of several electron transfer chain Fe-S enzymes or the protein level and activity of the tricarboxylic acid cycle aconitase (m-aconitase) (Fig. 7*D*). The only strong phenotypic alteration was a severe restriction of cell proliferation (Fig. 7*E*), as observed previously upon impairment of essential components of the ISC, export, and/or CIA machineries (39–41).

As shown above, the environment of the mNT cluster shares similar structural properties with that of ISCU (Fig. 3*B* and Ref. 42), and both proteins can transfer their cluster to bacterial apo-FDX (20, 43). However, using mNT with either apo-FDX from *Mastigocladus laminosus* (20) or *E. coli* (Fig. 8*A*), the Fe-S transfer reaction, which was followed by UV-visible absorption and a native PAGE mobility shift assay, occurs in aerobiosis, in contrast to the strict anoxia required for Fe-S transfer from ISCU to apo-FDX. These findings indicate that mNT, unlike ISCU, might function under oxidative conditions.

In mammals, the bifunctional cytosolic aconitase/IRP1 (c-aconitase) readily commutes from a [4Fe-4S]-containing form with aconitase activity to an apo-form with RNA-binding activity upon exposure to NO (44, 45) or H_2O_2 (46). Interestingly, the effect of NO and H_2O_2 is reversible, and the apo-form of IRP1 can recycle into c-aconitase (47–49), implying a still poorly defined cellular Fe-S repair pathway.

The first step was to prepare human purified holo-IRP1 and to trigger Fe-S cluster disassembly by NO (45) prior to using it as a recipient protein in an Fe-S transfer reaction with holo-mNT (Fig. 8*B*, *left panel*). As shown in Fig. 8*B*, *right panel*, holo-mNT was able to reactivate apo-IRP1 into a [4Fe-4S] aconitase in a time-dependent manner. We also observed that IRP1 reactivation by holo-mNT was as effective as chemical Fe-S reconstitution performed under the same conditions. In parallel, spontaneous Fe-S release of mNT was barely detectable under the conditions used for IRP1 reactivation by mNT. Moreover, when holo-mNT was replaced by fully disassembled mNT, the process of reactivation of apo-IRP1 into c-aconitase was barely perceptible. Together, these results strongly suggest that the *in vitro* reactivation of apo-IRP1 into holo-aconitase by mNT is carried out by direct Fe-S transfer rather than Fe-S disassembly/reassembly.

We then performed experiments on living cells and showed that endogenous mNT is stable in NO- and H_2O_2-treated cells and that the holo-form of mNT is maintained after exposure to NO and a bolus of H_2O_2 *in vitro* using native gel electrophoresis (Fig. 9*A*). Specifically, we showed that the cluster signature of mNT is unaffected after NO or H_2O_2 exposure (Fig. 9*B*). This contrasted with that of m-aconitase, a protein highly sensitive to oxidative stress (Fig. 9*C*). Furthermore, the cluster stability of H_2O_2- or NO-treated mNT was also very similar to that of untreated protein (Fig. 9*D*). These findings suggest that the peculiar Fe-S of mNT is resistant to H_2O_2 and NO and that mNT can serve as an escape protein to repair oxidatively damaged Fe-S proteins. Then, we investigated the role of mNT in the reassembly process of Fe-S into apo-IRP1 in living cells after H_2O_2 or NO exposure. In control and mNT-depleted cells, exogenous H_2O_2 inhibited c-aconitase activity as described previously (48, 49) without decreasing the IRP1 protein level. After the oxidative challenge with H_2O_2 of mNT-expressing cells, we observed a progressive reactivation of c-aconitase

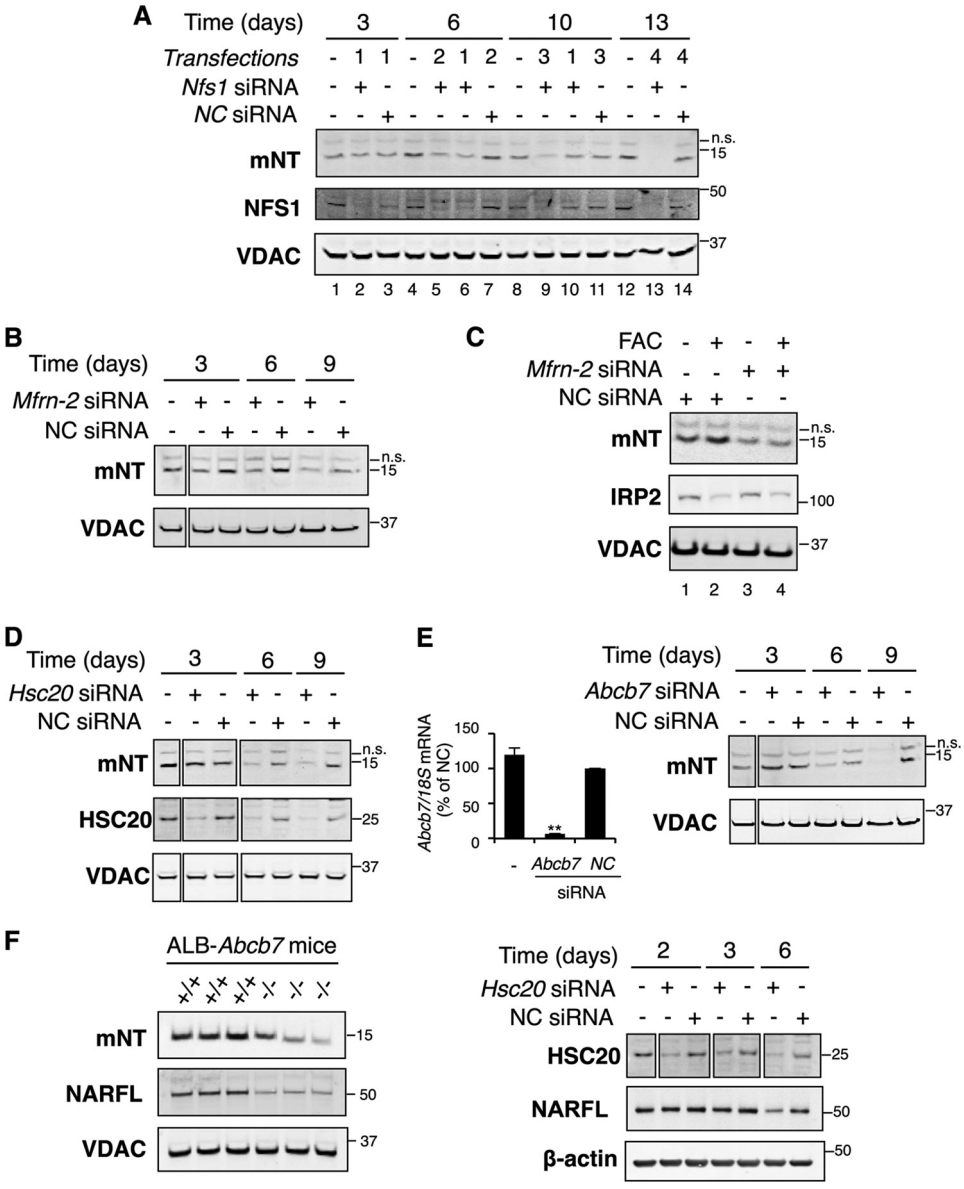

FIGURE 4. **Mitochondrial origin of the mNT Fe-S cluster.** *A*, total protein extracts from untransfected and *Nfs1* siRNA- or NC siRNA-transfected HeLa cells cultured for the indicated times were analyzed by immunoblotting using anti-mNT, anti-NFS1, and anti-VDAC antibodies. Silencing was either transitory with one single transfection (*lanes 2*, *6*, and *10*) or maintained for up to 13 days with two, three, or four rounds of siRNA transfections (*lanes 5*, *9*, and *13*). *n.s.*, nonspecific. *B*, untransfected, *Mfrn-2*-silenced, and NC siRNA-transfected cells were cultured for the indicated times, and mNT and VDAC protein levels were analyzed by immunoblotting. *C*, *Mfrn-2*-silenced and NC siRNA-transfected cells were cultured for 2 days in the presence of or without FAC, and total protein extracts were analyzed by immunoblotting using anti-mNT, anti-IRP2, and anti-VDAC antibodies. *D*, HeLa cells were either left untransfected or transfected with *Hsc20* or NC siRNAs. At the indicated times after transfection, total cell extracts were prepared and analyzed by immunoblotting using anti-mNT, anti-HSC20, and anti-VDAC antibodies. *E*, *left panel*, the mRNA level of *Abcb7* was determined by quantitative real-time PCR in untransfected (−) HeLa cells or 24 h after a single transfection with *Abcb7* or NC siRNA. Data were normalized to 18 S mRNA level for each strain and represented as a percentage of NC ± S.D. **, $p < 0.01$. *Right panel*, total protein extracts of *Abcb7* and NC siRNA-transfected cells cultured for the indicated times (days) were analyzed by immunoblotting using anti-mNT and anti-VDAC antibodies. *F*, total liver protein extracts from 4-week-old wild-type and ALB-*Abcb7*$^{lv/Y}$ mice (*left panel*) and total protein extracts from HSC20-depleted cells (*right panel*) were analyzed by immunoblot using anti-mNT, anti-NARFL, anti-VDAC, and anti-β-actin antibodies.

activity, whereas the latter was slowed significantly in mNT-depleted cells (Fig. 10*A*). In addition, the protein level of IRP2, which is regulated by the cytosolic iron concentration (29), was similar to that of control cells during H_2O_2 exposure and removal. We also exposed cells to NO to trigger Fe-S disassembly in c-aconitase/IRP1, as testified by the absence of IRP1 aconitase activity without a decrease in protein level (Fig. 10*B*, *left graph* and *blot*). As early as 1 h after NO removal, reactivation of IRP1 aconitase activity in control cells was detectable in HeLa cells, although with some degree of variability between samples. Nevertheless, each experiment, handled individually, showed diminished reactivation in mNT knockdown cells (data not shown). Furthermore, the ratio of recovery between control (taken as 100%) and mNT-deficient cells indicated a significant loss of reactivation upon mNT deficiency (Fig. 10*B*, *right graph*).

In parallel, we investigated the fate of GPAT and NARFL, whose apo-forms are prone to degradation. We found a consistent decrease of both protein levels independently of mNT knockdown in NO-treated cells, indicating an NO-mediated

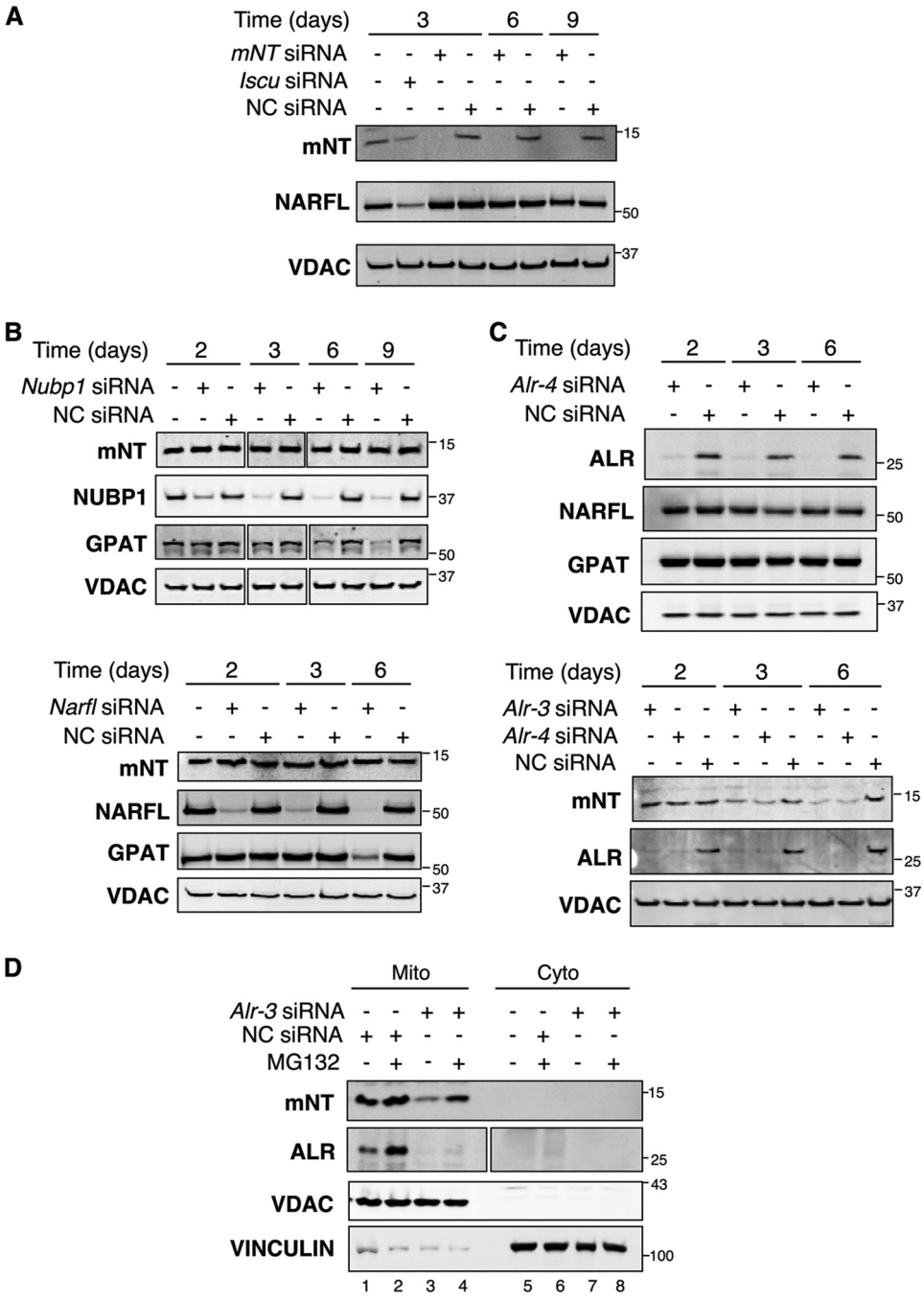

FIGURE 5. **The maturation of the mNT Fe-S cluster is independent of the CIA and requires a specific pathway involving HSC20/ABCb7/ALR.** Total protein extracts from HeLa cells left untransfected or transfected with *mNT* and *Iscu* siRNA (*A*), *Nubp1* siRNA (*B*, *top panel*), *NarfL* siRNA (*B*, *bottom panel*), two different *Alr* siRNA (*Alr-3* and *Alr-4*) (*C*), and NC siRNAs (*A*, *B*, and *C*) for the indicated times were analyzed by immunoblotting using antibodies against mNT, NUBP1, NARFL, ALR, GPAT, and VDAC. *D*, HeLa cells were transfected with *Alr-3* or NC siRNA for 8 days and then treated or not treated with MG132 for 18 additional hours. Cells were then fractionated into mitochondrial (*Mito*) and cytosolic (*Cyto*) fractions that were analyzed by immunoblotting using anti-mNT and anti-ALR antibodies. Fraction purity was assessed using antibodies against VDAC as a mitochondrial marker and vinculin as a cytosolic marker.

Fe-S cluster disassembly followed by protein degradation (Fig. 10*B*, *blot*). During the recovery phase after NO removal, GPAT and NARFL levels were kept low in both control and mNT-deficient cells. These findings reveal that, unlike c-aconitase/IRP1, GPAT, and NARFL, whose peptide stability depends on the presence of the cluster, cannot be repaired by mNT after stressful conditions. Together, these findings reveal a novel pathway involving mNT, independent of the classic CIA-dependent Fe-S cluster biogenesis pathway, and assigned to Fe-S cluster repair of the cytosolic aconitase/IRP1.

DISCUSSION

In this study, we address the process of maturation of mNT Fe-S and its function in the mammalian Fe-S repair pathway. By performing loss-of-function studies using human cells and animal models as well as biochemical and spectroscopic analyses, we disclosed the existence of an unrecognized mNT-dependent

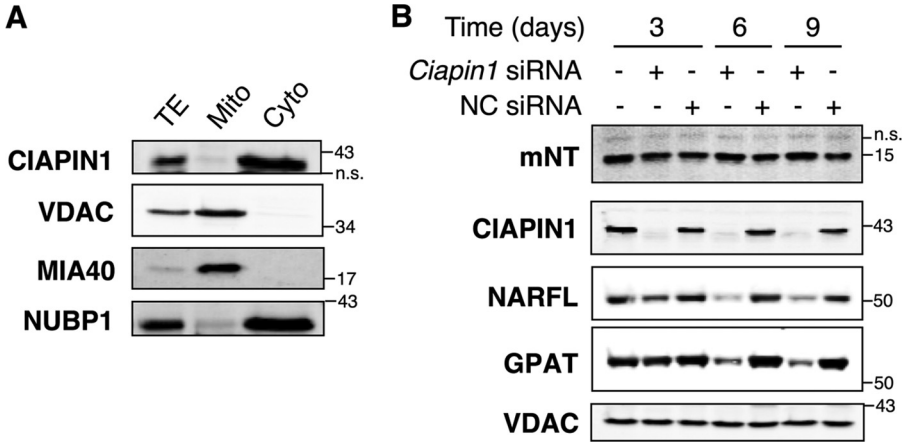

FIGURE 6. **CIAPIN1 is dispensable for mNT maturation but essential for the CIA component NARFL and cytosolic Fe-S GPAT.** *A*, total protein extracts (*TE*) from human HepG2 cells as well as purified cytosol (*Cyto*) and enriched mitochondrial fractions (*Mito*) were loaded onto an SDS-PAGE gel and analyzed by immunoblotting using anti-CIAPIN1 antibody. Fraction purity was assessed using antibodies against VDAC and MIA40 (mitochondrial markers) and NUBP1 (cytosolic marker). *n.s.*, nonspecific. *B*, total protein extracts from *ciapin1*-silenced and NC siRNA-transfected HeLa cells cultured for the indicated times were analyzed by immunoblotting using anti-mNT, anti-CIAPIN1, anti-NARFL, anti-GPAT, and anti-VDAC antibodies.

Fe-S branch pathway assigned to repair the master iron regulator c-aconitase/IRP1 (Fig. 11).

NMR and UV-visible spectroscopic analyses showed that mNT can cycle between an unstructured apo-form and a well folded [2Fe-2S] form, therefore underlining its structural plasticity. It is worth mentioning that the metamorphic scaffold protein IscU from *E. coli* also alternates between two conformations: a disordered state and a largely structured state that is stabilized by Fe-S cluster binding (50). Meanwhile, we also observed that mNT requires sustained activities of the mitochondrial ISC and export machineries with regard to the Fe-S supply to escape long lasting unstructured and proteasomal degradation. Along this line, it has been reported recently that the scaffold protein Isu is posttranslationally regulated by the mitochondrial protease Pim1 (51).

We characterized the pathway leading to Fe-S insertion into mNT on the external side of the OMM and demonstrated that the iron and sulfur moieties required come exclusively from mitochondria; that the main components of both mitochondrial ISC and export machineries (ISCU, FXN, NFS1, HSC20, and ABCb7) are required, whereas the CIA components are not needed; and that ALR, an IMS sulfhydryl oxidase that is dispensable for Fe-S incorporation into CIA proteins and GPAT, is obligatory. We therefore propose that preassembled Fe-S in mitochondria are routed to the OMM through a branch off the classic maturation pathway to deliver Fe-S to mNT and, presumably, to other, yet to be identified recipient apo-proteins anchored to the OMM (Fig. 9). In our study, the Fe-S assembly mode of mNT was independent of human CIAPIN1, although both proteins share a similar CIA-independent Fe-S assembly mode (35). CIAPIN1, which is mainly expressed in the cytosol, seems to act as an early component of the CIA rather than as a protein relay for mNT Fe-S assembly. Accordingly, Dre2, the yeast homolog of CIAPIN1, was has been reported recently to be a cytosolic protein associated with the OMM (52). Interestingly, in yeast, Tah18, the partner of Dre2, was relocalized from the cytosol to mitochondria after oxidative stress (53). Therefore, although mNT maturation does not need CIAPIN1 under physiological conditions, this does not exclude that, under conditions of oxidative stress, CIAPIN1, with its partner NDOR1, may be recruited to the OMM to play a role in concert with mNT.

The fact that the CIA machinery is dispensable for mNT maturation, whereas mitochondrial ISC and export machineries as well as the iron importer Mfn-2 are required, argues in favor of an export of preformed mitochondrial Fe-S across mitochondrial membranes and the IMS rather than two distinct iron and sulfide export pathways. Interestingly, it has been proposed recently that GSH, a member of the export pathway (10), forms a stable complex with Fe-S clusters, $[[Fe_2S_2]^{2+}(GS^-)_4]^{2-}$, which may deliver Fe-S to target proteins, in particular ABCb7 (54, 55). Such a small and stable nonprotein-bound GSH·Fe-S complex that can probably exit mitochondria through MTP proteins (56), therefore, constitutes a plausible candidate for Fe-S delivery to mNT.

In vitro, mNT is capable of transferring its cluster to bacterial [2Fe-2S] FDX (Ref. 20) and this study). However, the physiological apo-acceptor of mNT has not yet been identified. The fact that mNT transfers its [2Fe-2S] only in the presence of oxygen suggests that mNT activity is boosted under oxidative conditions. Meanwhile, we noticed that holo-mNT is not degraded by a bolus of H_2O_2 or NO flux, therefore enabling mNT to trigger the Fe-S transfer reaction after oxidative insults in living cells. Reactive oxygen species (ROS) and reactive nitrogen species are produced in many physiological and pathophysiological settings (57), including immune response and inflammation, and mammalian cells in the environment of ROS/reactive nitrogen species have to cope with their potential toxicity. We and others showed previously that the iron regulator c-aconitase/IRP1 possesses a [4Fe-4S] cluster that is readily disassembled upon reaction with redox mediators like NO or ROS produced upon immune response or inflammation (44, 58, 59). Interestingly, apo-IRP1 rapidly recovers initial aconitase activity (holo-IRP1) when NO flux stops (47) and after H_2O_2 removal (49). The rather high stability of apo-IRP1 in an oxidative and nitrosative environment is compatible with a status of apo-acceptor of mNT Fe-S. Here we show that mNT helps resupply apo-IRP1 with a [4Fe-4S] cluster after an NO and/or

H_2O_2 challenge in living cells. Although alternate scenarios may also be considered, the mechanism of the recycling of apo-IRP1 into holo-aconitase by mNT seems to require direct Fe-S transfer in living cells and is not mediated by the cytosolic iron pool, as indicated by IRP2 stability during both the cellular H_2O_2 challenge and reactivation phase. Interestingly, the regulation of two other Fe-S proteins, GPAT and NARFL, contrasts with that of c-aconitase/IRP1 because NO-stimulated damage

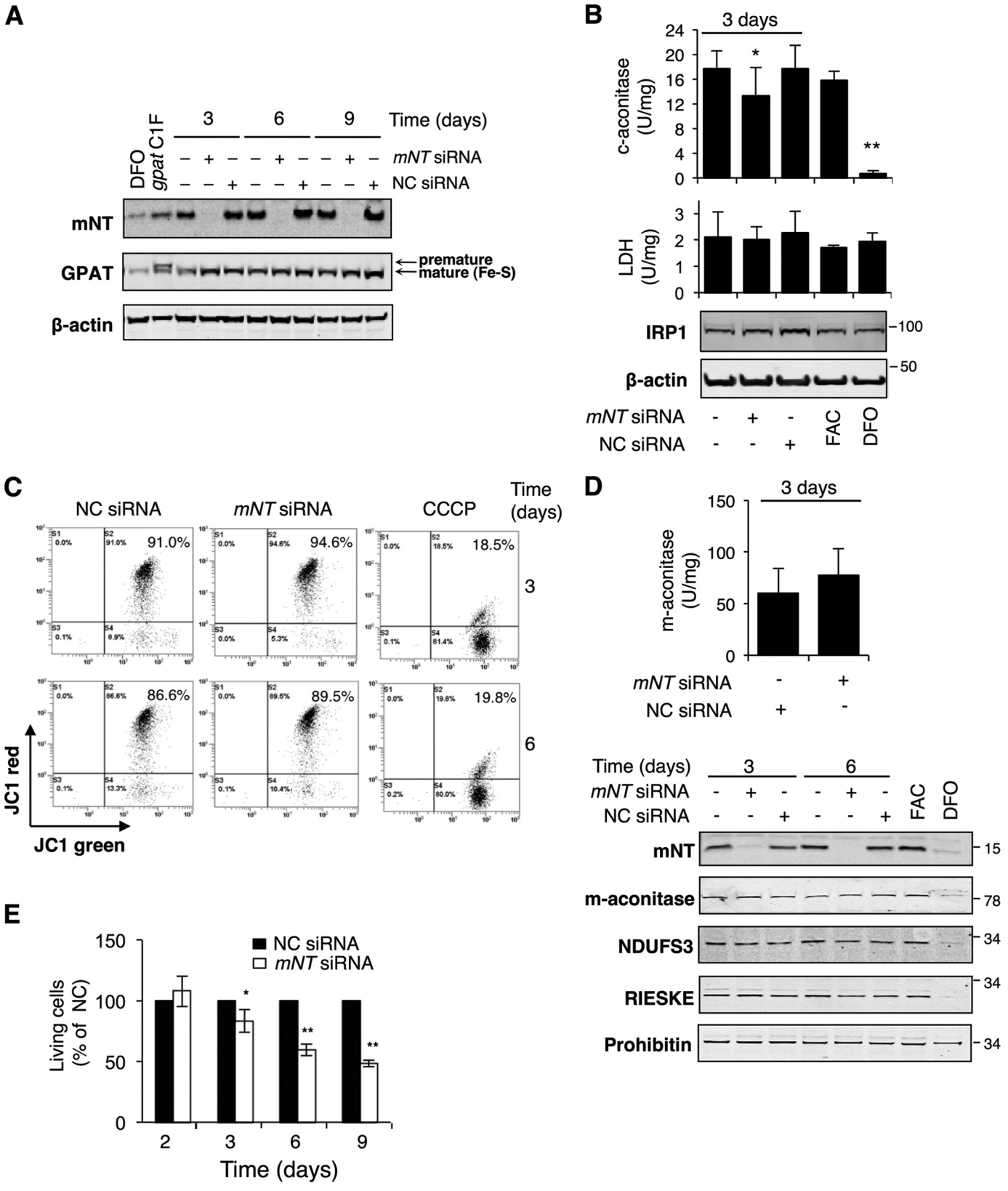

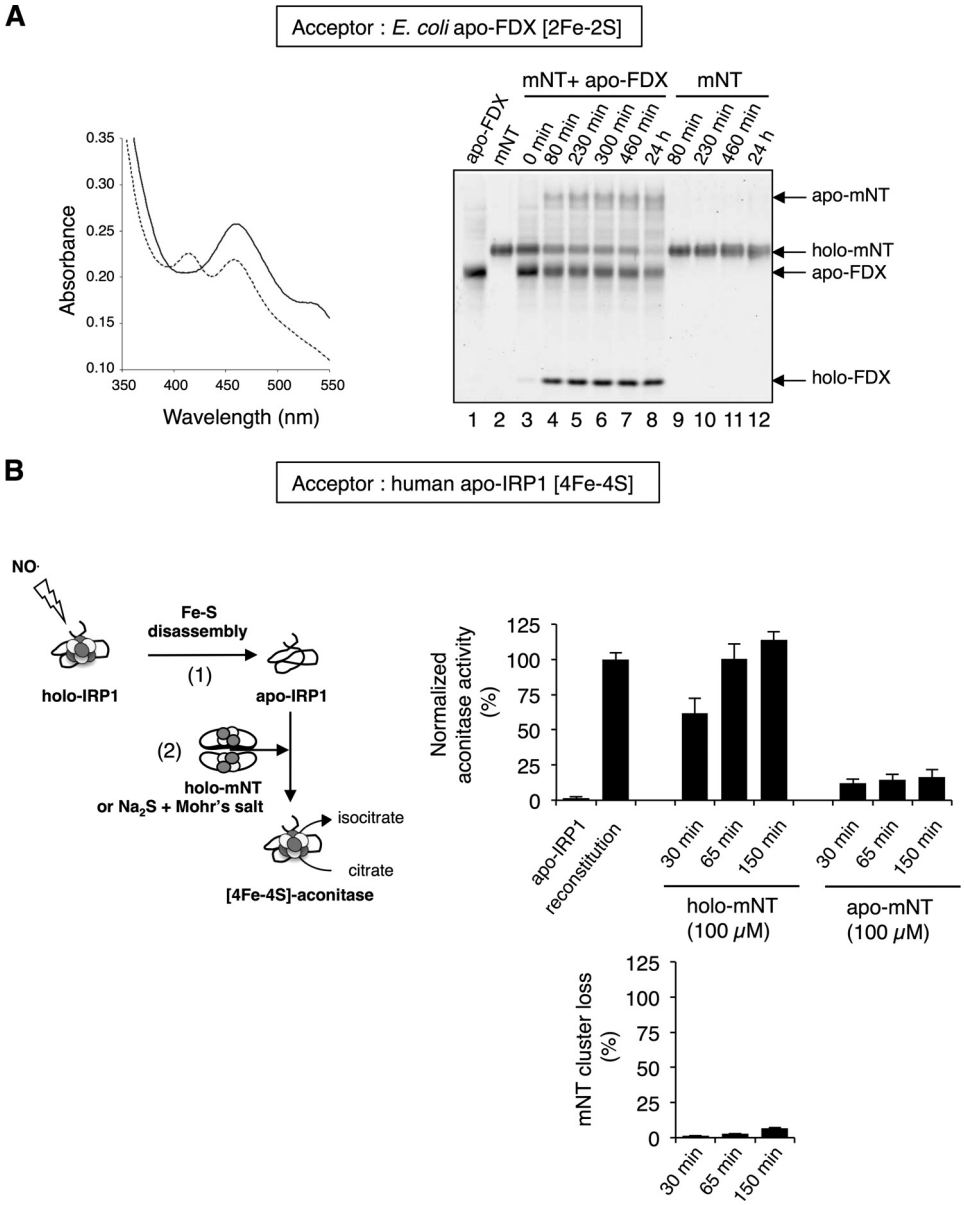

FIGURE 8. **Analysis of the Fe-S transfer reactions from holo-mNT to *E. coli* apo-FDX and to human apo-IRP1.** *A*, the reaction was performed at 20 °C (pH 6.2) using 50 μM holo-mNT and 50 μM apo-FDX in aerobiosis. *Left panel*, the initial UV-visible spectrum (*solid line*) of the reaction mixture, which contained apo-FDX and holo-mNT, showed the band at 458 nm, characteristic of holo-mNT. At the end of the reaction, the spectrum (*dotted line*) was markedly different, with a decrease of absorbance at 458 nm and the appearance of the band at 415 nm, characteristic of holo-FDX. *Right panel*, Fe-S cluster transfer followed by native gel shows the increase of holo-FDX and concomitant disappearance of holo-mNT. Note that holo-mNT, which was incubated alone under the same conditions as in the reaction transfer, is remarkably stable at pH 6.2 without protein acceptor (compare *lanes 4*, *5*, *7*, and *8* with lanes *9*, *10*, *11*, and *12*, respectively). *B*, *left panel*, schematic of the protocol for Fe-S cluster transfer studies. (*1*), apo-IRP1 is obtained by exposure of purified holo-IRP1 to NO gas in an anaerobic chamber. (*2*), 25 μM DTT-reduced apo-IRP1 was incubated with 100 μM human holo-mNT$_{44-108}$ (*100 μM holo-mNT*) or 100 μM disassembled mNT$_{44-108}$ (*100 μM apo-mNT*) or 250 μM Na_2S and Mohr's salt (reconstitution) in 100 mM BisTris (pH 6.2), 100 mM NaCl, and 5 mM DTT at 25 °C under anaerobic conditions. Aliquots of the reaction were removed at the indicated times, and aconitase activity was measured. *Right panel*, *top graph*, aconitase activity is expressed as a percentage of the activity obtained after chemical reconstitution performed under the same buffer conditions (means ± S.D., $n > 3$). *Bottom graph*, mNT cluster loss was studied under the same conditions and calculated by monitoring the decrease of absorbance at 460 nm over time.

FIGURE 7. **mNT deficiency inhibits cell proliferation and mildly affects cytosolic aconitase activity.** HeLa cells were transfected for the indicated times with *mNT* or NC siRNA or treated overnight under iron-loaded (FAC) or iron-deprived (DFO) conditions. Cells were analyzed directly (*C* and *E*), lysed to obtain total cellular extracts (*A*), or fractionated to isolate the cytosolic (*B*) and mitochondrial fractions (*D*). *A*, total extracts from the same conditions as above or transfected in parallel with a vector expressing the uncleavable *gpat* mutant (*gpat C1F*) were subjected to electrophoresis and immunoblotted with antibodies against mNT, GPAT, and β-actin. *B*, activities of cytosolic aconitase (*IRP1*) (*top panel*, *top graph*; represented as means ± S.D.; $n = 11$; *, $p < 0.05$; **, $p < 0.001$) and lactate dehydrogenase (*LDH*) (*top panel*, *top graph*, means ± S.D., $n = 3$) in cytosolic fractions. *Bottom panel*, the IRP1 protein level was analyzed by immunoblotting with β-actin as a loading control. *C*, flow cytometry analysis was used to measure the mitochondrial membrane potential using JC-1 dye. The mitochondrial uncoupling agent carbonyl cyanide 3-chlorophenylhydrazone (*CCCP*, 200 μM) was used as a positive control. D, the specific activity of mitochondrial aconitase was measured in mitochondria-enriched fractions of *mNT* and NC siRNA-transfected at the indicated times (means ± S.D., $n = 4$). *Bottom panel*, protein levels of mNT, mitochondrial aconitase, NDUFS3 (Fe-S subunit of complex I), RIESKE (Fe-S subunit of complex III) and prohibitin (used as a loading control) were determined by immunoblotting in total extracts. *E*, cells were stained with trypan blue dye to exclude dead cells, and the uncolored living cells were counted and are represented in the graph as a percentage of NC siRNA-transfected cells ± S.D. *, $p < 0.05$; **, $p < 0.001$ ($n = 3$).

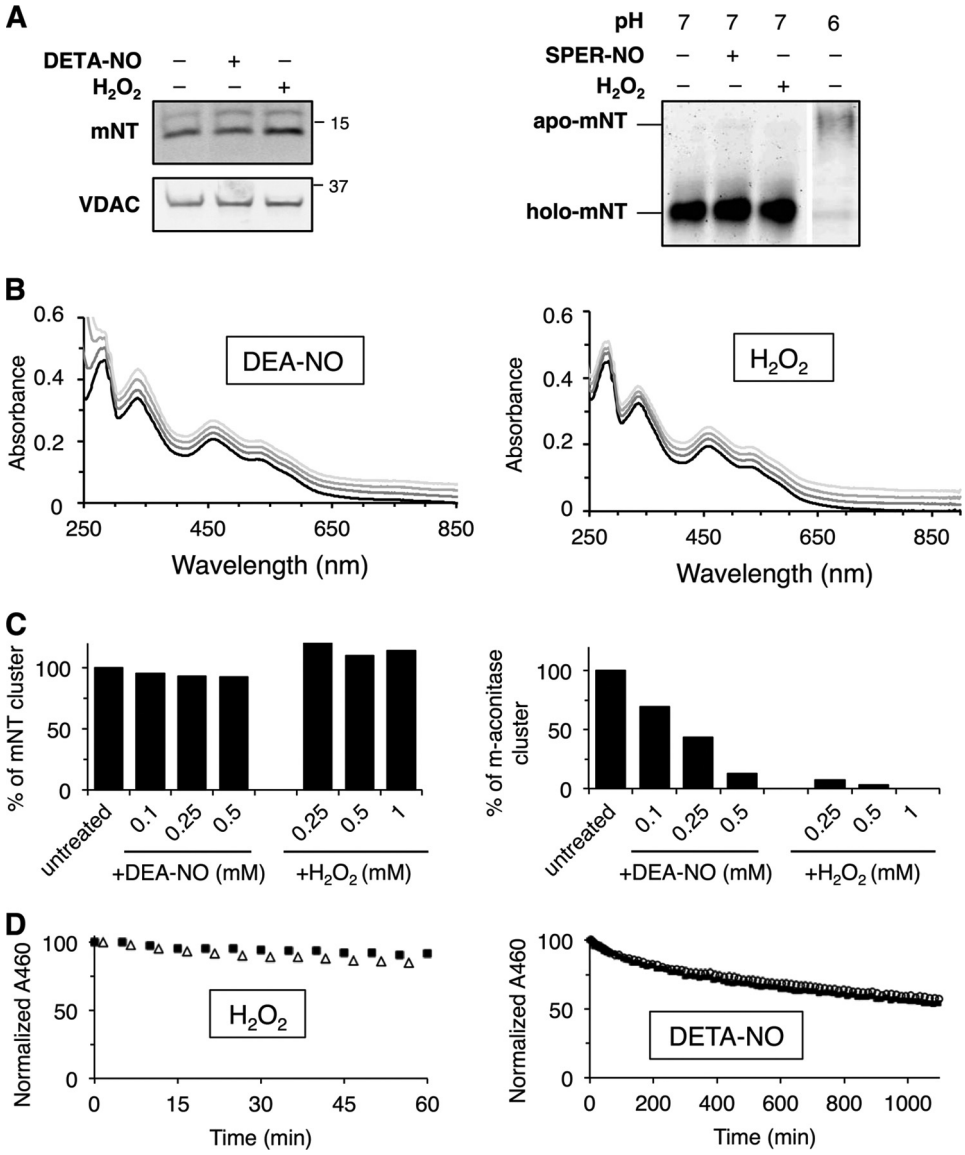

FIGURE 9. **The mNT Fe-S cluster is stable after NO and H_2O_2 exposure *in vitro* and in living cells.** *A*, *left panel*, immunoblotting of mNT and VDAC after electrophoresis of total extracts from HeLa cells left untreated and treated with DETA-NO for 16 h or H_2O_2 for 1 h. *Right panel*, purified holo-mNT was incubated or not incubated with spermine-nitric oxide complex (*SPER-NO*) or H_2O_2 for 3 h at 37 °C (see "Experimental Procedures" for details) and loaded on a native gel in parallel to apo-mNT obtained by incubating mNT under aerobic conditions for 10 min at 65 °C (pH 6). *B*, UV-visible spectra of a solution containing 30 μM holo-mNT in 50 mM Tris (pH 7.2), 100 mM NaCl were recorded after 20 min of incubation at 37 °C with increasing concentrations of DEA-NO (*left panel*) and H_2O_2 (*right panel*). Absorbances were corrected for the baseline at 900 nm, and then curves for H_2O_2/DEA-NO treatments were shifted by 0.02, 0,04, and 0.06 from the lowest to the highest concentrations for the clarity of the figure. *Black lines*, untreated protein; *dark gray lines*, 100 μM DEA-NO or 250 μM H_2O_2; *gray lines*, 250 μM DEA-NO or 500 μM H_2O_2; *light gray lines*, 500 μM DEA-NO or 1 mM H_2O_2. *C*, comparison of the stability of mNT and m-aconitase Fe-S clusters after DEA-NO or H_2O_2 treatment as in *B*. The ratio of absorbances at 460 and 280 nm was calculated from the experiments presented in *B* and then normalized for the value obtained for the untreated protein (100% of mNT cluster). M-aconitase (30 μM) was treated similarly with DEA-NO or H_2O_2, and then aconitase activity (directly linked to the presence of the [4Fe-4S] cluster) was measured and expressed relative to the activity of the untreated protein. *D*, change in absorbance at 460 nm over time of a 50 mM Tris solution (pH 7.2), 100 mM NaCl containing 30 μM holo-mNT in the absence of treatment (■), or after treatment with 250 μM H_2O_2 (△, *left panel*) or 250 μM DETA-NO (○, *right panel*). Absorbances were normalized by the absorbance at the beginning of the reaction. In each case, the duration of the treatment was similar to that used in the experiments in living cells (*A*).

of their clusters renders their apo-form unstable. Therefore, GPAT and NARFL cannot be targets of mNT. Recovery of these two unstable proteins very likely requires *de novo* synthesis and Fe-S traffic along the classic Fe-S biogenesis pathway.

By *in vitro* studies, we also showed that [2Fe-2S] mNT was able to reactivate a purified apo-IRP-1 whose [4Fe-4S] cluster was disassembled previously by NO into an active aconitase under anaerobic conditions. This implies an interconversion of two planar [2Fe-2S] to a cubane [4Fe-4S], as described previously in *in vitro* studies showing activation of bacterial apo-aconitase (AcoA) by the bacterial ISC scaffold proteins IscA/SufA (60–62). Our findings are also consistent with recent data showing that *Azotobacter vinelandii* ^{Nif}IscA, a member of the A-type proteins that are required for repair of [4Fe-4S] proteins (63–65), accommodates a [2Fe-2S] cluster upon oxygen exposure or under oxidative stress conditions (66).

We observed that siRNA depletion of mNT is more effective on repair of IRP1 than on its maturation. This implies that apo-IRP1 left after ROS- or NO-mediated Fe-S extrusion is different from the neosynthesized form. As outlined previously,

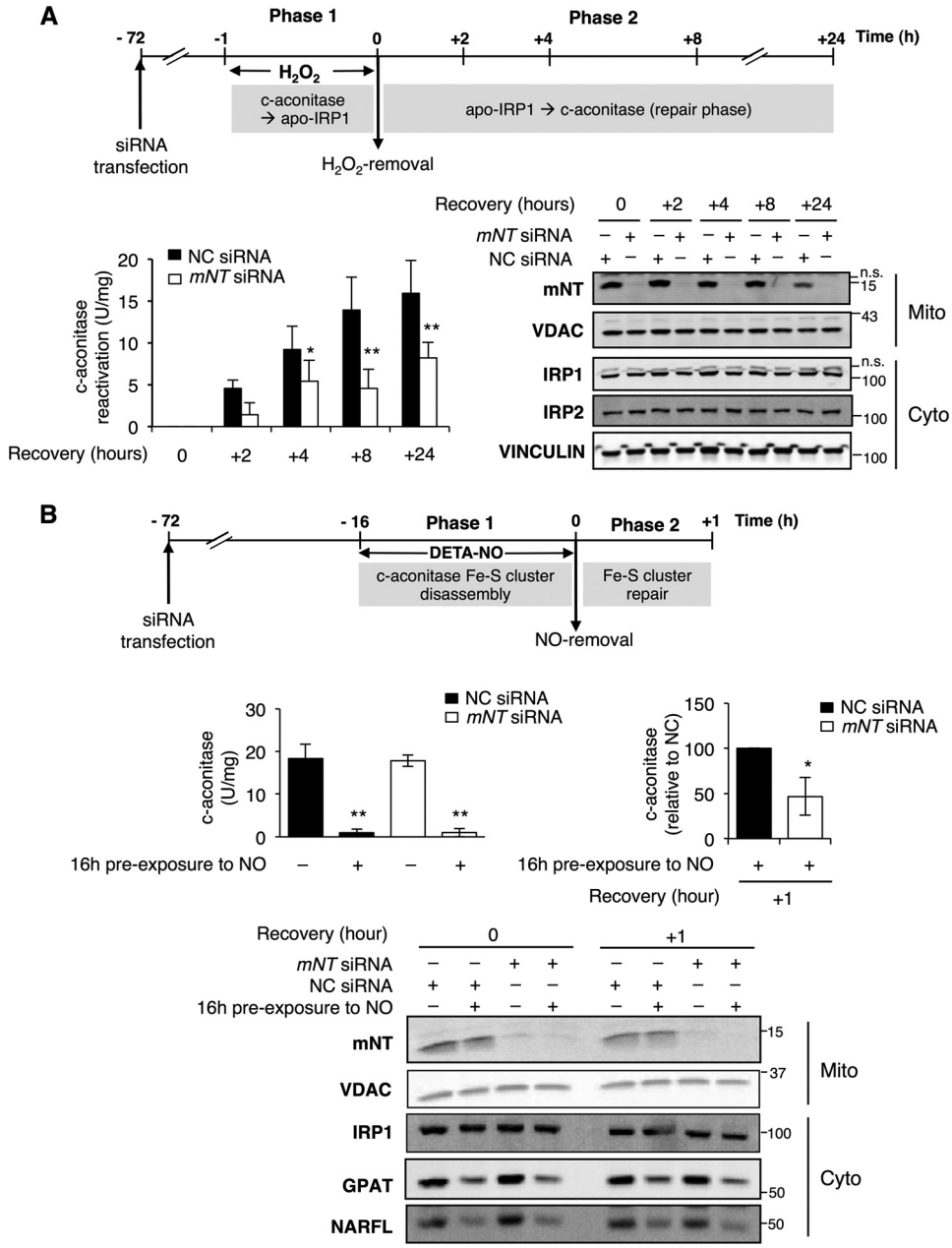

FIGURE 10. **mNT is required to restore the cytosolic aconitase activity of IRP1 after H_2O_2 and NO challenge.** *A*, *top panel* and *bottom left panel*, HeLa cells transfected with *mNT* or NC siRNA for 72 h were exposed to a bolus of H_2O_2 (150 μM) for 1 h. Cells were then washed (time 0) and incubated further in fresh culture medium for the indicated additional hours. Pure cytosolic extracts were obtained at 0 (*Phase 1*) and at 2, 4, 8, and 24 h (*Phase 2*, recovery) to analyze c-aconitase activity (means ± S.D.; $n = 5$; *, $p < 0.05$; **, $p < 0.001$). *Bottom right panel*, immunoblotting of mitochondrial and cytosolic protein extracts using antibodies against mNT, IRP1 and IRP2, respectively. Antibodies against VDAC and vinculin were used as loading controls. *n.s.*, nonspecific; *Cyto*, cytosolic fraction; *Mito*, mitochondrial fraction. *B*, *top panel*, HeLa cells transfected with *mNT* or NC siRNA for 72 h were exposed to DETA-NO for 16 h. NO was then removed by washing (time 0), and cells were incubated further in fresh culture medium for an additional hour. Pure cytosolic extracts were obtained at 0 h (*Phase 1*) and 1 h after NO removal (*Phase 2*, recovery) to analyze the cytosolic aconitase activity. *Center panel*, *left*, activities of cytosolic aconitase (*IRP1*) at time 0 h (phase 1), represented as means ± S.D. ($n = 4$). **, $p < 0.001$. *Center panel*, *right*, relative activity of cytosolic aconitase at time 1 h after NO removal (phase 2). Results are presented as the ratio of c-aconitase recovery for *mNT*-depleted cells over NC cells ± S.D. ($n = 4$). *, $p < 0.05$. *Bottom panel*, immunoblotting of mitochondrial and cytosolic extracts using antibodies against mNT, VDAC, IRP1, GPAT, and NARFL.

protein-bound [4Fe-4S] display noticeable modifications in the Fe-S binding site upon oxygen-mediated Fe-S disassembly, notably persulfuration (67–69). Therefore, we speculate that cysteine persulfuration on apo-IRP1 following exposure to oxygen or nitrogen species favors mNT Fe-S delivery. We propose that mNT is an adaptive repair enzyme whose activity depends on cellular redox balance. Interestingly, two protein sensors of redox and iron homeostasis, IscR and Grx3–4/Fra2, have been shown recently to have the same unusual Cys_3-His_1-ligated [2Fe-2S] cluster of mNT (70, 71).

IRP1 is a master regulator of cellular iron homeostasis and HIF-2α-dependent erythropoiesis (72, 73). Besides, mNT deficiency in both white adipose tissue and liver leads to higher concentrations of mitochondrial iron compared with wild-type mice (12). Accordingly, limiting Fe-S reassembly in IRP1 by mNT deficiency and thereby maintaining its *trans*-regulatory

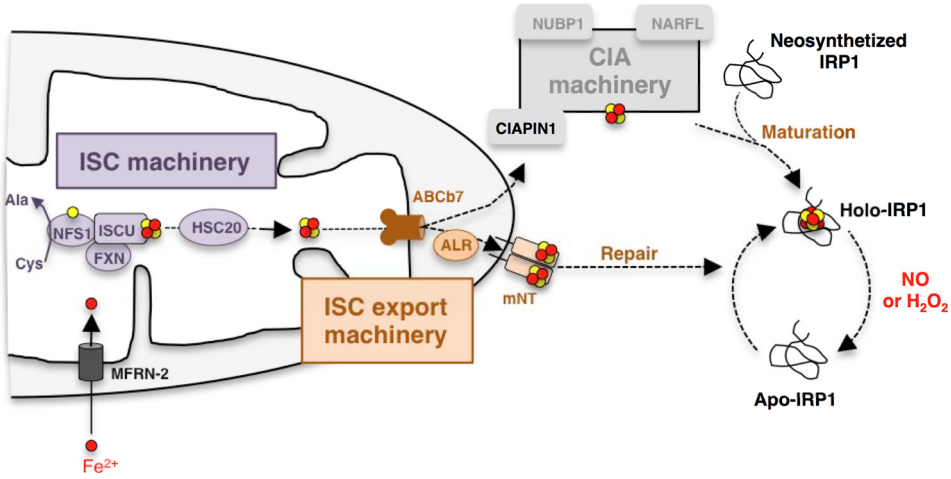

FIGURE 11. **Proposed schematic for the maturation of mNT and its role in exporting mitochondrial Fe-S and reactivating the cytosolic apo-IRP1 into Fe-S aconitase after H_2O_2-induced oxidative and nitrosative stress.** In this model, the components of the ISC (*purple*), export (*brown*), and CIA (*gray*) machineries shown are limited to those addressed in this study. Fe-S of mNT is built with mitochondrial ferrous iron imported by the inner membrane carrier MFRN-2 and sulfur provided by NFS1. The mitochondrial ISCU and FXN platform, on which a transiently bound Fe-S is formed, is required for mNT maturation, along with the HSC20 chaperone, which facilitates the release of ISCU-bound Fe-S. In the inner mitochondrial membrane/IMS, ABCb7 and ALR constitute a maturation pathway dedicated to mNT Fe-S assembly that functions independently of the CIA members CIAPIN1, NUBP1, and NARFL. When mature, holo-mNT in a reducing environment is stable and does not contribute to maturation of extramitochondrial Fe-S proteins. Upon NO and H_2O_2 exposure, the cytosolic holo-aconitase is activated into the RNA-binding form of IRP1 (apo-form) through Fe-S disassembly. After NO or H_2O_2 challenge, holo-mNT can recycle the cytosolic apo-IRP1 into holo-aconitase through an Fe-S transfer process without passing through the CIA machinery.

function, may help supply mitochondria with iron and, consequently, regulate the mitochondrial electron transport chain. Along this line of thought, it is known that although both IRP1 and IRP2 provide a proper supply of iron to mitochondria to secure mitochondrial function (74), only IRP1 ensures adequate iron levels for restoring mitochondrial aconitase activity after stressful treatments (75). Iron (38) and mNT (12) have also been shown to regulate, in an opposite way, the expression of the insulin-sensitizing hormone adiponectin, which contributes to the suppression of metabolic syndrome in type 2 diabetes. Our study supports the view that the missing element linking mNT, intracellular iron concentrations, and adiponectin is its physiological target IRP1. There is major interest in understanding how mammalian cells convey Fe-S from the mitochondrion to the other cell compartments. This is of particular relevance for cell-like immune cells or hepatocytes that have to cope with high levels of ROS or NO and must adapt promptly to oxidative/nitrosative damage.

Acknowledgments—We are grateful to Dr. Jean-Marc Moulis (CEA, Grenoble, France) for the purified holo-IRP1, Dr. Eric Jacquet for the help with protein purification, and Dr. Jérome Bignon at ICSN for assistance with flow cytometry. We also thank Cendrine Seguin for assistance with quantitative RT-PCR; Dr. Nelly Morellet for help with NMR; Dr. Benoît D'Autréaux for expertise in biophysical analysis; Laurence Reutenauer for generating and genotyping all mice used in this study; Adrien Tereygeol, Safa Khelifi, and Héla Allani for technical support. We also acknowledge the IMAGIF cloning platform (CNRS, 91198 Gif-sur-Yvette, France).

REFERENCES

1. Sheftel, A., Stehling, O., and Lill, R. (2010) Iron-sulfur proteins in health and disease. *Trends Endocrinol. Metab.* **21,** 302–314
2. Shaw, G. C., Cope, J. J., Li, L., Corson, K., Hersey, C., Ackermann, G. E., Gwynn, B., Lambert, A. J., Wingert, R. A., Traver, D., Trede, N. S., Barut, B. A., Zhou, Y., Minet, E., Donovan, A., Brownlie, A., Balzan, R., Weiss, M. J., Peters, L. L., Kaplan, J., Zon, L. I., and Paw, B. H. (2006) Mitoferrin is essential for erythroid iron assimilation. *Nature* **440,** 96–100
3. Puccio, H., Simon, D., Cossée, M., Criqui-Filipe, P., Tiziano, F., Melki, J., Hindelang, C., Matyas, R., Rustin, P., and Koenig, M. (2001) Mouse models for Friedreich ataxia exhibit cardiomyopathy, sensory nerve defect and Fe-S enzyme deficiency followed by intramitochondrial iron deposits. *Nat. Genet.* **27,** 181–186
4. Shi, Y., Ghosh, M., Kovtunovych, G., Crooks, D. R., and Rouault, T. A. (2012) Both human ferredoxins 1 and 2 and ferredoxin reductase are important for iron-sulfur cluster biogenesis. *Biochim. Biophys. Acta* **1823,** 484–492
5. Uhrigshardt, H., Singh, A., Kovtunovych, G., Ghosh, M., and Rouault, T. A. (2010) Characterization of the human HSC20, an unusual DnaJ type III protein, involved in iron-sulfur cluster biogenesis. *Hum. Mol. Genet.* **19,** 3816–3834
6. Camaschella, C., Campanella, A., De Falco, L., Boschetto, L., Merlini, R., Silvestri, L., Levi, S., and Iolascon, A. (2007) The human counterpart of zebrafish shiraz shows sideroblastic-like microcytic anemia and iron overload. *Blood* **110,** 1353–1358
7. Sharma, A. K., Pallesen, L. J., Spang, R. J., and Walden, W. E. (2010) Cytosolic iron-sulfur cluster assembly (CIA) system: factors, mechanism, and relevance to cellular iron regulation. *J. Biol. Chem.* **285,** 26745–26751
8. Cavadini, P., Biasiotto, G., Poli, M., Levi, S., Verardi, R., Zanella, I., Derosas, M., Ingrassia, R., Corrado, M., and Arosio, P. (2007) RNA silencing of the mitochondrial ABCB7 transporter in HeLa cells causes an iron-deficient phenotype with mitochondrial iron overload. *Blood* **109,** 3552–3559
9. Lange, H., Lisowsky, T., Gerber, J., Mühlenhoff, U., Kispal, G., and Lill, R. (2001) An essential function of the mitochondrial sulfhydryl oxidase Erv1p/ALR in the maturation of cytosolic Fe/S proteins. *EMBO Rep.* **2,** 715–720
10. Sipos, K., Lange, H., Fekete, Z., Ullmann, P., Lill, R., and Kispal, G. (2002) Maturation of cytosolic iron-sulfur proteins requires glutathione. *J. Biol. Chem.* **277,** 26944–26949
11. Kumar, C., Igbaria, A., D'Autreaux, B., Planson, A. G., Junot, C., Godat, E., Bachhawat, A. K., Delaunay-Moisan, A., and Toledano, M. B. (2011) Glutathione revisited: a vital function in iron metabolism and ancillary role in thiol-redox control. *EMBO J.* **30,** 2044–2056
12. Kusminski, C. M., Holland, W. L., Sun, K., Park, J., Spurgin, S. B., Lin, Y., Askew, G. R., Simcox, J. A., McClain, D. A., Li, C., and Scherer, P. E. (2012)

MitoNEET-driven alterations in adipocyte mitochondrial activity reveal a crucial adaptive process that preserves insulin sensitivity in obesity. *Nat. Med.* **18,** 1539–1549
13. Colca, J. R., McDonald, W. G., Waldon, D. J., Leone, J. W., Lull, J. M., Bannow, C. A., Lund, E. T., and Mathews, W. R. (2004) Identification of a novel mitochondrial protein ("mitoNEET") cross-linked specifically by a thiazolidinedione photoprobe. *Am. J. Physiol. Endocrinol. Metab.* **286,** E252–E260
14. Colca, J. R., McDonald, W. G., Cavey, G. S., Cole, S. L., Holewa, D. D., Brightwell-Conrad, A. S., Wolfe, C. L., Wheeler, J. S., Coulter, K. R., Kilkuskie, P. M., Gracheva, E., Korshunova, Y., Trusgnich, M., Karr, R., Wiley, S. E., Divakaruni, A. S., Murphy, A. N., Vigueira, P. A., Finck, B. N., and Kletzien, R. F. (2013) Identification of a mitochondrial target of thiazolidinedione insulin sensitizers (mTOT)-relationship to newly identified mitochondrial pyruvate carrier proteins. *PLoS ONE* **8,** e61551
15. Hou, X., Liu, R., Ross, S., Smart, E. J., Zhu, H., and Gong, W. (2007) Crystallographic studies of human MitoNEET. *J. Biol. Chem.* **282,** 33242–33246
16. Lin, J., Zhou, T., Ye, K., and Wang, J. (2007) Crystal structure of human mitoNEET reveals distinct groups of iron sulfur proteins. *Proc. Natl. Acad. Sci. U.S.A.* **104,** 14640–14645
17. Paddock, M. L., Wiley, S. E., Axelrod, H. L., Cohen, A. E., Roy, M., Abresch, E. C., Capraro, D., Murphy, A. N., Nechushtai, R., Dixon, J. E., and Jennings, P. A. (2007) MitoNEET is a uniquely folded 2Fe 2S outer mitochondrial membrane protein stabilized by pioglitazone. *Proc. Natl. Acad. Sci. U.S.A.* **104,** 14342–14347
18. Wiley, S. E., Paddock, M. L., Abresch, E. C., Gross, L., van der Geer, P., Nechushtai, R., Murphy, A. N., Jennings, P. A., and Dixon, J. E. (2007) The outer mitochondrial membrane protein mitoNEET contains a novel redox-active 2Fe-2S cluster. *J. Biol. Chem.* **282,** 23745–23749
19. Wiley, S. E., Murphy, A. N., Ross, S. A., van der Geer, P., and Dixon, J. E. (2007) MitoNEET is an iron-containing outer mitochondrial membrane protein that regulates oxidative capacity. *Proc. Natl. Acad. Sci. U.S.A.* **104,** 5318–5323
20. Zuris, J. A., Harir, Y., Conlan, A. R., Shvartsman, M., Michaeli, D., Tamir, S., Paddock, M. L., Onuchic, J. N., Mittler, R., Cabantchik, Z. I., Jennings, P. A., and Nechushtai, R. (2011) Facile transfer of [2Fe-2S] clusters from the diabetes drug target mitoNEET to an apo-acceptor protein. *Proc. Natl. Acad. Sci. U.S.A.* **108,** 13047–13052
21. Thierbach, R., Schulz, T. J., Isken, F., Voigt, A., Mietzner, B., Drewes, G., von Kleist-Retzow, J. C., Wiesner, R. J., Magnuson, M. A., Puccio, H., Pfeiffer, A. F., Steinberg, P., and Ristow, M. (2005) Targeted disruption of hepatic frataxin expression causes impaired mitochondrial function, decreased life span and tumor growth in mice. *Hum. Mol. Genet.* **14,** 3857–3864
22. Pondarré, C., Antiochos, B. B., Campagna, D. R., Clarke, S. L., Greer, E. L., Deck, K. M., McDonald, A., Han, A. P., Medlock, A., Kutok, J. L., Anderson, S. A., Eisenstein, R. S., and Fleming, M. D. (2006) The mitochondrial ATP-binding cassette transporter Abcb7 is essential in mice and participates in cytosolic iron-sulfur cluster biogenesis. *Hum. Mol. Genet.* **15,** 953–964
23. Martelli, A., Wattenhofer-Donzé, M., Schmucker, S., Bouvet, S., Reutenauer, L., and Puccio, H. (2007) Frataxin is essential for extramitochondrial Fe-S cluster proteins in mammalian tissues. *Hum. Mol. Genet.* **16,** 2651–2658
24. Guillon, B., Bulteau, A. L., Wattenhofer-Donzé, M., Schmucker, S., Friguet, B., Puccio, H., Drapier, J. C., and Bouton, C. (2009) Frataxin deficiency causes upregulation of mitochondrial Lon and ClpP proteases and severe loss of mitochondrial Fe-S proteins. *FEBS J.* **276,** 1036–1047
25. Ferecatu, I., Bergeaud, M., Rodríguez-Enfedaque, A., Le Floch, N., Oliver, L., Rincheval, V., Renaud, F., Vallette, F. M., Mignotte, B., and Vayssière, J. L. (2009) Mitochondrial localization of the low level p53 protein in proliferative cells. *Biochem. Biophys. Res. Commun.* **387,** 772–777
26. Drapier, J. C., and Hibbs, J. B., Jr. (1996) Aconitases: a class of metalloproteins highly sensitive to nitric oxide synthesis. *Methods Enzymol.* **269,** 26–36
27. Ta, D. T., and Vickery, L. E. (1992) Cloning, sequencing, and overexpression of a [2Fe-2S] ferredoxin gene from *Escherichia coli*. *J. Biol. Chem.* **267,** 11120–11125
28. Carboni, M., Clémancey, M., Molton, F., Pécaut, J., Lebrun, C., Dubois, L., Blondin, G., and Latour, J. M. (2012) Biologically relevant heterodinuclear iron-manganese complexes. *Inorg. Chem.* **51,** 10447–10460
29. Anderson, C. P., Shen, M., Eisenstein, R. S., and Leibold, E. A. (2012) Mammalian iron metabolism and its control by iron regulatory proteins. *Biochim. Biophys. Acta* **1823,** 1468–1483
30. Ciesielski, S. J., Schilke, B. A., Osipiuk, J., Bigelow, L., Mulligan, R., Majewska, J., Joachimiak, A., Marszalek, J., Craig, E. A., and Dutkiewicz, R. (2012) Interaction of J-protein co-chaperone Jac1 with Fe-S scaffold Isu is indispensable *in vivo* and conserved in evolution. *J. Mol. Biol.* **417,** 1–12
31. Shan, Y., and Cortopassi, G. (2012) HSC20 interacts with frataxin and is involved in iron-sulfur cluster biogenesis and iron homeostasis. *Hum. Mol. Genet.* **21,** 1457–1469
32. Balk, J., Pierik, A. J., Netz, D. J., Mühlenhoff, U., and Lill, R. (2004) The hydrogenase-like Nar1p is essential for maturation of cytosolic and nuclear iron-sulphur proteins. *EMBO J.* **23,** 2105–2115
33. Fischer, M., and Riemer, J. (2013) The mitochondrial disulfide relay system: roles in oxidative protein folding and beyond. *Int. J. Cell Biol.* **2013,** 742923
34. Mühlenhoff, U., Molik, S., Godoy, J. R., Uzarska, M. A., Richter, N., Seubert, A., Zhang, Y., Stubbe, J., Pierrel, F., Herrero, E., Lillig, C. H., and Lill, R. (2010) Cytosolic monothiol glutaredoxins function in intracellular iron sensing and trafficking via their bound iron-sulfur cluster. *Cell Metab.* **12,** 373–385
35. Netz, D. J., Stümpfig, M., Doré, C., Mühlenhoff, U., Pierik, A. J., and Lill, R. (2010) Tah18 transfers electrons to Dre2 in cytosolic iron-sulfur protein biogenesis. *Nat. Chem. Biol.* **6,** 758–765
36. Banci, L., Bertini, I., Ciofi-Baffoni, S., Boscaro, F., Chatzi, A., Mikolajczyk, M., Tokatlidis, K., and Winkelmann, J. (2011) Anamorsin is a [2Fe-2S] cluster-containing substrate of the Mia40-dependent mitochondrial protein trapping machinery. *Chem. Biol.* **18,** 794–804
37. Zhang, Y., Lyver, E. R., Nakamaru-Ogiso, E., Yoon, H., Amutha, B., Lee, D. W., Bi, E., Ohnishi, T., Daldal, F., Pain, D., and Dancis, A. (2008) Dre2, a conserved eukaryotic Fe/S cluster protein, functions in cytosolic Fe/S protein biogenesis. *Mol. Cell Biol.* **28,** 5569–5582
38. Gabrielsen, J. S., Gao, Y., Simcox, J. A., Huang, J., Thorup, D., Jones, D., Cooksey, R. C., Gabrielsen, D., Adams, T. D., Hunt, S. C., Hopkins, P. N., Cefalu, W. T., and McClain, D. A. (2012) Adipocyte iron regulates adiponectin and insulin sensitivity. *J. Clin. Invest.* **122,** 3529–3540
39. Fosset, C., Chauveau, M. J., Guillon, B., Canal, F., Drapier, J. C., and Bouton, C. (2006) RNA silencing of mitochondrial m-Nfs1 reduces Fe-S enzyme activity both in mitochondria and cytosol of mammalian cells. *J. Biol. Chem.* **281,** 25398–25406
40. Biederbick, A., Stehling, O., Rösser, R., Niggemeyer, B., Nakai, Y., Elsässer, H. P., and Lill, R. (2006) Role of human mitochondrial Nfs1 in cytosolic iron-sulfur protein biogenesis and iron regulation. *Mol. Cell Biol.* **26,** 5675–5687
41. Stehling, O., Netz, D. J., Niggemeyer, B., Rösser, R., Eisenstein, R. S., Puccio, H., Pierik, A. J., and Lill, R. (2008) Human Nbp35 is essential for both cytosolic iron-sulfur protein assembly and iron homeostasis. *Mol. Cell Biol.* **28,** 5517–5528
42. Chandramouli, K., Unciuleac, M. C., Naik, S., Dean, D. R., Huynh, B. H., and Johnson, M. K. (2007) Formation and properties of [4Fe-4S] clusters on the IscU scaffold protein. *Biochemistry* **46,** 6804–6811
43. Chandramouli, K., and Johnson, M. K. (2006) HscA and HscB stimulate [2Fe-2S] cluster transfer from IscU to apoferredoxin in an ATP-dependent reaction. *Biochemistry* **45,** 11087–11095
44. Bouton, C., and Drapier, J. C. (2003) Iron regulatory proteins as NO signal transducers. *Sci. STKE*, pe17
45. Soum, E., Brazzolotto, X., Goussias, C., Bouton, C., Moulis, J. M., Mattioli, T. A., and Drapier, J. C. (2003) Peroxynitrite and nitric oxide differently target the iron-sulfur cluster and amino acid residues of human iron regulatory protein 1. *Biochemistry* **42,** 7648–7654
46. Pantopoulos, K., and Hentze, M. W. (1995) Rapid responses to oxidative stress mediated by iron regulatory protein. *EMBO J.* **14,** 2917–2924
47. Bouton, C., Chauveau, M. J., Lazereg, S., and Drapier, J. C. (2002) Recycling of RNA binding iron regulatory protein 1 into an aconitase after nitric

oxide removal depends on mitochondrial ATP. *J. Biol. Chem.* **277,** 31220–31227
48. Pantopoulos, K., Weiss, G., and Hentze, M. W. (1996) Nitric oxide and oxidative stress (H_2O_2) control mammalian iron metabolism by different pathways. *Mol. Cell Biol.* **16,** 3781–3788
49. Tong, W. H., and Rouault, T. A. (2006) Functions of mitochondrial ISCU and cytosolic ISCU in mammalian iron-sulfur cluster biogenesis and iron homeostasis. *Cell Metab.* **3,** 199–210
50. Markley, J. L., Kim, J. H., Dai, Z., Bothe, J. R., Cai, K., Frederick, R. O., and Tonelli, M. (2013) Metamorphic protein IscU alternates conformations in the course of its role as the scaffold protein for iron-sulfur cluster biosynthesis and delivery. *FEBS Lett.* **587,** 1172–1179
51. Song, J. Y., Marszalek, J., and Craig, E. A. (2012) Cysteine desulfurase Nfs1 and Pim1 protease control levels of Isu, the Fe-S cluster biogenesis scaffold. *Proc. Natl. Acad. Sci. U.S.A.* **109,** 10370–10375
52. Peleh, V., Riemer, J., Dancis, A., and Herrmann, J. M. (2014) Protein oxidation in the intermembrane space of mitochondria is substrate-specific rather than general. *Microb. Cell* **1,** 81–93
53. Vernis, L., Facca, C., Delagoutte, E., Soler, N., Chanet, R., Guiard, B., Faye, G., and Baldacci, G. (2009) A newly identified essential complex, Dre2-Tah18, controls mitochondria integrity and cell death after oxidative stress in yeast. *PLoS ONE* **4,** e4376
54. Qi, W., Li, J., Chain, C. Y., Pasquevich, G. A., Pasquevich, A. F., and Cowan, J. A. (2012) Glutathione complexed Fe-S centers. *J. Am. Chem. Soc.* **134,** 10745–10748
55. Qi, W., Li, J., and Cowan, J. A. (2014) A structural model for glutathione-complexed iron-sulfur cluster as a substrate for ABCB7-type transporters. *Chem. Commun. (Camb.)* **50,** 3795–3798
56. Aniya, Y., and Imaizumi, N. (2011) Mitochondrial glutathione transferases involving a new function for membrane permeability transition pore regulation. *Drug Metab. Rev.* **43,** 292–299
57. Wink, D. A., Hines, H. B., Cheng, R. Y., Switzer, C. H., Flores-Santana, W., Vitek, M. P., Ridnour, L. A., and Colton, C. A. (2011) Nitric oxide and redox mechanisms in the immune response. *J. Leukocyte Biol.* **89,** 873–891
58. Fillebeen, C., and Pantopoulos, K. (2002) Redox control of iron regulatory proteins. *Redox Rep.* **7,** 15–22
59. Brazzolotto, X., Gaillard, J., Pantopoulos, K., Hentze, M. W., and Moulis, J. M. (1999) Human cytoplasmic aconitase (Iron regulatory protein 1) is converted into its [3Fe-4S] form by hydrogen peroxide *in vitro* but is not activated for iron-responsive element binding. *J. Biol. Chem.* **274,** 21625–21630
60. Unciuleac, M. C., Chandramouli, K., Naik, S., Mayer, S., Huynh, B. H., Johnson, M. K., and Dean, D. R. (2007) *In vitro* activation of apo-aconitase using a [4Fe-4S] cluster-loaded form of the IscU [Fe-S] cluster scaffolding protein. *Biochemistry* **46,** 6812–6821
61. Gupta, V., Sendra, M., Naik, S. G., Chahal, H. K., Huynh, B. H., Outten, F. W., Fontecave, M., and Ollagnier de Choudens, S. (2009) Native *Escherichia coli* SufA, coexpressed with SufBCDSE, purifies as a [2Fe-2S] protein and acts as an Fe-S transporter to Fe-S target enzymes. *J. Am. Chem. Soc.* **131,** 6149–6153
62. Tan, G., Lu, J., Bitoun, J. P., Huang, H., and Ding, H. (2009) IscA/SufA paralogues are required for the [4Fe-4S] cluster assembly in enzymes of multiple physiological pathways in *Escherichia coli* under aerobic growth conditions. *Biochem. J.* **420,** 463–472
63. Mühlenhoff, U., Richter, N., Pines, O., Pierik, A. J., and Lill, R. (2011) Specialized function of yeast Isa1 and Isa2 proteins in the maturation of mitochondrial [4Fe-4S] proteins. *J. Biol. Chem.* **286,** 41205–41216
64. Sheftel, A. D., Wilbrecht, C., Stehling, O., Niggemeyer, B., Elsässer, H. P., Mühlenhoff, U., and Lill, R. (2012) The human mitochondrial ISCA1, ISCA2, and IBA57 proteins are required for [4Fe-4S] protein maturation. *Mol. Biol. Cell* **23,** 1157–1166
65. Mapolelo, D. T., Zhang, B., Naik, S. G., Huynh, B. H., and Johnson, M. K. (2012) Spectroscopic and functional characterization of iron-bound forms of *Azotobacter vinelandii* (Nif)IscA. *Biochemistry* **51,** 8056–8070
66. Mapolelo, D. T., Zhang, B., Naik, S. G., Huynh, B. H., and Johnson, M. K. (2012) Spectroscopic and functional characterization of iron-sulfur cluster-bound forms of *Azotobacter vinelandii* (Nif)IscA. *Biochemistry* **51,** 8071–8084
67. Kennedy, M. C., and Beinert, H. (1988) The state of cluster SH and S2- of aconitase during cluster interconversions and removal: a convenient preparation of apoenzyme. *J. Biol. Chem.* **263,** 8194–8198
68. Zhang, B., Crack, J. C., Subramanian, S., Green, J., Thomson, A. J., Le Brun, N. E., and Johnson, M. K. (2012) Reversible cycling between cysteine persulfide-ligated [2Fe-2S] and cysteine-ligated [4Fe-4S] clusters in the FNR regulatory protein. *Proc. Natl. Acad. Sci. U.S.A.* **109,** 15734–15739
69. Nicolet, Y., Rohac, R., Martin, L., and Fontecilla-Camps, J. C. (2013) X-ray snapshots of possible intermediates in the time course of synthesis and degradation of protein-bound Fe4S4 clusters. *Proc. Natl. Acad. Sci. U.S.A.* **110,** 7188–7192
70. Fleischhacker, A. S., Stubna, A., Hsueh, K. L., Guo, Y., Teter, S. J., Rose, J. C., Brunold, T. C., Markley, J. L., Münck, E., and Kiley, P. J. (2012) Characterization of the [2Fe-2S] cluster of *Escherichia coli* transcription factor IscR. *Biochemistry* **51,** 4453–4462
71. Li, H., Mapolelo, D. T., Dingra, N. N., Naik, S. G., Lees, N. S., Hoffman, B. M., Riggs-Gelasco, P. J., Huynh, B. H., Johnson, M. K., and Outten, C. E. (2009) The yeast iron regulatory proteins Grx3/4 and Fra2 form heterodimeric complexes containing a [2Fe-2S] cluster with cysteinyl and histidyl ligation. *Biochemistry* **48,** 9569–9581
72. Anderson, S. A., Nizzi, C. P., Chang, Y. I., Deck, K. M., Schmidt, P. J., Galy, B., Damnernsawad, A., Broman, A. T., Kendziorski, C., Hentze, M. W., Fleming, M. D., Zhang, J., and Eisenstein, R. S. (2013) The IRP1-HIF-2α axis coordinates iron and oxygen sensing with erythropoiesis and iron absorption. *Cell Metab.* **17,** 282–290
73. Wilkinson, N., and Pantopoulos, K. (2013) IRP1 regulates erythropoiesis and systemic iron homeostasis by controlling HIF2α mRNA translation. *Blood* **122,** 1658–1668
74. Galy, B., Ferring-Appel, D., Sauer, S. W., Kaden, S., Lyoumi, S., Puy, H., Kölker, S., Gröne, H. J., and Hentze, M. W. (2010) Iron regulatory proteins secure mitochondrial iron sufficiency and function. *Cell Metab.* **12,** 194–201
75. Styś, A., Galy, B., Starzyński, R. R., Smuda, E., Drapier, J. C., Lipiński, P., and Bouton, C. (2011) Iron regulatory protein 1 outcompetes iron regulatory protein 2 in regulating cellular iron homeostasis in response to nitric oxide. *J. Biol. Chem.* **286,** 22846–22854